Structural Elements in Domain IV that Influence Biophysical and Pharmacological Properties of Human α_{1A}-Containing High-Voltage-Activated Calcium Channels

M. Hans, A. Urrutia, C. Deal, P. F. Brust, K. Stauderman, S. B. Ellis, M. M. Harpold, E. C. Johnson, and M. E. Williams
SIBIA Neurosciences, Inc., La Jolla, California 92037-4641 USA

ABSTRACT We have cloned two splice variants of the human homolog of the α_{1A} subunit of voltage-gated Ca^{2+} channels. The sequences of human $\alpha_{1A\text{-}1}$ and $\alpha_{1A\text{-}2}$ code for proteins of 2510 and 2662 amino acids, respectively. Human $\alpha_{1A\text{-}2}\alpha_{2b}\delta\beta_{1b}$ Ca^{2+} channels expressed in HEK293 cells activate rapidly ($\tau_{+10mV} = 2.2$ ms), deactivate rapidly ($\tau_{-90mV} = 148$ μs), inactivate slowly ($\tau_{+10mV} = 690$ ms), and have peak currents at a potential of +10 mV with 15 mM Ba^{2+} as charge carrier. In HEK293 cells transient expression of Ca^{2+} channels containing $\alpha_{1A/B(f)}$, an α_{1A} subunit containing a 112 amino acid segment of $\alpha_{1B\text{-}1}$ sequence in the IVS3-IVSS1 region, resulted in Ba^{2+} currents that were 30-fold larger compared to wild-type (wt) $\alpha_{1A\text{-}2}$-containing Ca^{2+} channels, and had inactivation kinetics similar to those of $\alpha_{1B\text{-}1}$-containing Ca^{2+} channels. Cells transiently transfected with $\alpha_{1A/B(f)}\alpha_{2b}\delta\beta_{1b}$ expressed higher levels of the α_1, $\alpha_{2b}\delta$, and β_{1b} subunit polypeptides as detected by immunoblot analysis. By mutation analysis we identified two locations in domain IV within the extracellular loops S3-S4 ($N^{1655}P^{1656}$) and S5-SS1 (E^{1740}) that influence the biophysical properties of α_{1A}. α_{1A}E1740R resulted in a threefold increase in current magnitude, a −10 mV shift in steady-state inactivation, and an altered Ba^{2+} current inactivation, but did not affect ion selectivity. The deletion mutant $\alpha_{1A}\Delta$NP shifted steady-state inactivation by −20 mV and increased the fast component of current inactivation twofold. The potency and rate of block by ω-Aga IVA was increased with $\alpha_{1A}\Delta$NP. These results demonstrate that the IVS3-S4 and IVS5-SS1 linkers play an essential role in determining multiple biophysical and pharmacological properties of α_{1A}-containing Ca^{2+} channels.

INTRODUCTION

Voltage-gated Ca^{2+} channels play important roles in neurotransmitter release, excitation-contraction coupling, hormone secretion, and a variety of other physiological processes. Based on biophysical and pharmacological criteria, multiple types of Ca^{2+} channels have been identified in intact neurons (L-, T-, N-, R-, and P/Q-type; Hofmann et al., 1994; Hess, 1990; Tsien et al., 1991; Swandulla et al., 1991; Snutch and Reiner, 1992). Consistent with these observations, molecular cloning and expression studies have identified at least five genes expressed in the nervous system that encode the pore-forming α_1 subunit, termed α_{1A}, α_{1B}, α_{1C}, α_{1D}, and α_{1E} (for review see Snutch and Reiner, 1992; Birnbaumer et al., 1994). The α_{1A} gene encodes the pore-forming subunit of a high-voltage-activated Ca^{2+} channel that is sensitive to ω-Aga IVA and ω-CTx MVIIC (Mori et al., 1991; Sather et al., 1993). The α_{1A} subunit has also been shown to interact with the neuronal β subunits β_{1b}, β_2, β_3, or β_4 (Liu et al., 1996), and these β subunits have been shown to change biophysical properties of the α_{1A} subunit (De Waard and Campbell, 1995). These properties, and the distribution of α_{1A} RNA and protein in mammalian brain, suggest that P-type Ca^{2+} channels in cerebellar Purkinje neurons and the Q-type Ca^{2+} channels in cerebellar granular cells may contain the α_{1A} subunit (Starr et al., 1991; Llinas et al., 1992; Mintz et al., 1992a, b; Randall and Tsien, 1995; Sather et al., 1993; Stea et al., 1994; Westenbroek et al., 1995; Tottene et al., 1996). However, the biophysical and pharmacological properties of P- and Q-type and recombinant α_{1A}-containing Ca^{2+} channels do not precisely correlate; this discrepancy might be a result of differences in their structure and subunit composition.

Recent studies indicate that the levels of functional expression of recombinant Ca^{2+} channels can differ significantly. For example, functional expression of recombinant Ca^{2+} channels containing rat α_{1B} in *Xenopus* oocytes is relatively poor compared to those containing a rabbit α_{1A} subunit (Mori et al., 1991; Ellinor et al., 1994). We found that human $\alpha_{1B\text{-}1}$-containing Ca^{2+} channels can be expressed efficiently in HEK293 cells, as indicated by the number of ω-CgTx-GVIA binding sites and robust current magnitude (Brust et al., 1993; Williams et al., 1992), whereas functional expression of human $\alpha_{1A\text{-}2}$-containing Ca^{2+} channels in HEK293 cells is markedly lower.

In this work we describe the cloning of cDNAs encoding two structural variants of the human α_{1A} Ca^{2+} channel subunit and examine biophysical properties of the $\alpha_{1A\text{-}2}$ variant in combination with human $\alpha_{2b}\delta$ and β_{1b} subunits in HEK293 cells. In addition, we constructed $\alpha_{1A/B}$ chimeras and α_{1A} mutations to identify regions in the α_{1A} subunit amino acid sequence that control current magnitude, gating properties, and sensitivity to ω-Aga IVA. Preliminary com-

Received for publication 20 August 1998 and in final form 7 December 1998.

Address reprint requests to Michael Hans, SIBIA Neurosciences, 505 Coast Blvd. South, Suite 300, La Jolla, CA 92037-4641. Tel.: 619-452-5892 ext. 423; Fax: 619-452-9279; E-mail: mhans@sibia.com.

0006-3495/99/03/1384/17 $2.00

munications of some of this work have been published (Zahl et al., 1994; Williams et al., 1995).

MATERIALS AND METHODS

cDNA libraries

Recombinant cDNA libraries were prepared in the phage vector λgt10 essentially as described (Gubler and Hoffman, 1983; Lapeyre and Amalric, 1985). Two human cerebellum libraries were constructed from poly(A+)-selected RNA: 1) random-primed, >1.0 kb, and 2) specifically primed (primer is the complement of human α_{1A} nt 2485 to 2510), >2.0 kb.

Isolation of cDNAs

Approximately 2×10^6 recombinants of the random-primed library were screened with a combination of oligonucleotide probes based on the rat α_{1A} sequence: oligonucleotide 1, complementary to rat nt 767 to 796; oligonucleotide 2, rat nt 2288 to 2315; oligonucleotide 3, rat nt 3559 to 3585; oligonucleotide 4, rat nt 4798 to 4827; and oligonucleotide 5, rat nt 6190 to 6217. Clones 1.244 (human nt 5131 to 7555), 1.254 (human nt 5686 to ~8400), 1.274 (human nt 2287 to 4001), and 1.278 (human nt 2871 to 4968) were identified and characterized. Oligonucleotides 1 and 2 were used to screen $\sim 8 \times 10^5$ recombinants of the specifically primed library. Clone 1.381 (human nt −236 to 2510) was isolated and characterized. All cDNAs were subcloned into pGEM7Z (Promega, Madison, WI). The DNA sequence was determined by the dideoxy chain-termination method using Sequenase 2.0 (USB, Cleveland, OH) or with an Applied Biosystems 373A automated DNA sequencer and the Taq DyeDeoxy terminator cycle sequencing kit (Applied Biosystems, Foster City, CA).

Full-length construct

To facilitate the construction of a full-length α_{1A} cDNA, two fragments were amplified from human cerebellum total RNA by polymerase chain reaction (PCR). pcDNA$\alpha_{1A\text{-}1}$ was constructed in pcDNA1 (Invitrogen, San Diego, CA) using α1.381 (nt −236 to 2267), PCR fragment 1 (nt 2267 to 2879), α1.278 (nt 2879 to 4939), PCR fragment 2 (nt 4939 to 5282), and α1.244 (nt 5282 to 7555). For pcDNA$\alpha_{1A\text{-}2}$ the *Bgl*II/*Sal*I fragment of α1.254 ($\alpha_{1A\text{-}2}$ nt 5879 to 7143) replaced the corresponding α1.244 fragment.

Chimera/mutation constructions

The full-length α_{1A} (pcDNA$\alpha_{1A\text{-}2}$) and α_{1B} (pcDNA$\alpha_{1B\text{-}1}$) constructs were described previously and are denoted in this section as $\alpha_{1A\text{-}2}$ and $\alpha_{1B\text{-}1}$, respectively. Chimeras between $\alpha_{1A\text{-}2}$ and $\alpha_{1B\text{-}1}$ in the pcDNA1 expression vector (Invitrogen, San Diego, CA) are designated $\alpha_{1A/B(a)}$–$\alpha_{1A/B(f)}$ and were constructed as follows:

$\alpha_{1A/B(a)}$: A PCR primer containing the mutations C5232G and A5233C that creates an *Sph*I site in the $\alpha_{1B\text{-}1}$ sequence was used to amplify a fragment of $\alpha_{1B\text{-}1}$ from 5217 to 5622. An *Sph*I(5233)-*Kpn*I(5525) fragment of the PCR product and a *Kpn*I(5525)-*Xba*I(7177) fragment of $\alpha_{1B\text{-}1}$ were introduced into $\alpha_{1A\text{-}2}$ at the unique *Sph*I(5557)-*Xba*I (3′ polylinker) sites.

$\alpha_{1A/B(b)}$: A *Bam*HI (5′ polylinker)-*Kpn*I (4459A) fragment of $\alpha_{1A\text{-}2}$ was ligated into the *Bam*HI (5′ polylinker)-*Kpn*I (5304B) sites of $\alpha_{1B\text{-}1}$.

$\alpha_{1A/B(c)}$: A PCR primer with mutation T4650C creating an *Eco*RV site in the $\alpha_{1B\text{-}1}$ sequence was used to amplify a fragment of $\alpha_{1B\text{-}1}$ from 4632 to 5334. An *Eco*RV-*Xho*I (5304) fragment of the PCR product and an *Xho*I-*Xba*I fragment of $\alpha_{1B\text{-}1}$ were introduced into the corresponding region of $\alpha_{1A\text{-}2}$ at the unique *Eco*RV (4942) and *Xba*I (3′ polylinker) sites.

$\alpha_{1A/B(d)}$: PCR primers with mutation T4650C creating an *Eco*RV site in addition to C5232G and A5233C creating an *Sph*I site in the $\alpha_{1B\text{-}1}$ sequence were used to amplify a fragment of $\alpha_{1B\text{-}1}$ from 4632 to 5244. The PCR product was introduced into the corresponding region of $\alpha_{1A\text{-}2}$ at the unique *Eco*RV (4942) and *Sph*I (5557) sites.

$\alpha_{1A/B(e)}$: PCR primers with mutations G4965A and C4968T creating a *Hin*DIII site in addition to C5232G and A5233C creating an *Sph*I site in the $\alpha_{1B\text{-}1}$ sequence were used to amplify a fragment of $\alpha_{1B\text{-}1}$ from 4957 to 5244. The PCR product was introduced into the corresponding region of $\alpha_{1A\text{-}2}$ at the unique *Hin*DIII (5283) and *Sph*I (5557) sites.

$\alpha_{1A/B(f)}$: Mutagenic PCR primers with mutation T4650C creating an *Eco*RV site in addition to G4965A and C4968T creating a *Hin*DIII site in the $\alpha_{1B\text{-}1}$ sequence were used to amplify a fragment of $\alpha_{1B\text{-}1}$ from 4632 to 4980. The PCR product was introduced into the corresponding region of $\alpha_{1A\text{-}2}$ at the unique *Eco*RV (4942) and *Hin*DIII (5283) sites.

Individual point mutations were made using PCR. For the $\alpha_{1A\text{-}2}$ mutations partially overlapping, complementary PCR primers containing the silent mutation G5205A and introducing an *Eco*RI site in the $\alpha_{1A\text{-}2}$ sequence were used to direct the amplification of two adjoining $\alpha_{1A\text{-}2}$ fragments encompassing nts 4928–5211 and 5200–5751. One of the fragments also contained the desired point mutation. The two fragments were ligated into the unique *Eco*RV (4942) and *Sph*I (5557) sites of $\alpha_{1A\text{-}2}$. For the $\alpha_{1B\text{-}1}$ mutation, a mutagenic PCR primer was used to amplify a fragment of $\alpha_{1B\text{-}1}$ from nt 4860–5334. An *Sph*I (4870)-*Xho*I (5304) fragment of the PCR product was introduced into the SspI and *Xho*I sites of $\alpha_{1B\text{-}1}$. All chimeras and point mutations were confirmed by DNA sequencing. The ΔNP construct was generated by the overlap extension method of the PCR (Ho et al., 1989). An *Eco*RV (4942)–*Hin*DIII (5283) fragment containing deletion of nucleotides 4963–4968 was ligated into *Eco*RV and *Hin*DIII sites of $\alpha_{1A\text{-}2}$.

Expression

All human α_1 subunit cDNAs [wild-type (wt), chimera, mutants] were transiently coexpressed with human $\alpha_{2b}\delta$ and β_{1b} subunit cDNAs in HEK293 cells. Transfections were performed using a standard calcium phosphate-mediated procedure as described previously (Williams et al., 1994; Brust et al., 1993).

Immunoblot analysis

Total membrane fractions were prepared essentially as described elsewhere (Perez-Reyes et al., 1989). Briefly, cells from five or six 10-cm dishes were rinsed with ice-cold, 50 mM Tris/pH 7.2, 1 mM EDTA, resuspended in 12 ml of the rinse buffer supplemented with a cocktail of protease inhibitors (PI) containing aprotinin (2.0 μg/ml), leupeptin (2.0 μg/ml), pepstatin (2.0 μg/ml), benzamidine HCl (4.0 mM), calpain inhibitor I (5 μg/ml), calpain inhibitor II (5.0 μg/ml), and phenylmethylsulfonyl fluoride (500 μM) and homogenized in a Kontes glass/Teflon homogenizer (15 strokes). The suspension was centrifuged at $400 \times g$ for 5 min at 4°C. The pellet was resuspended in 12 ml ice-cold buffer/PI, rehomogenized, and recentrifuged. The supernatants from the two low-speed spins were combined and centrifuged at $100{,}000 \times g$ for 30 min at 4°C. The pellet was resuspended in 0.5 ml of 50 mM Tris/pH 7.2, 1 mM EDTA, PI. The total yield of membrane protein was typically 2–3 mg.

Proteins were separated by SDS-PAGE on 4–12% gradient gels and transferred to nitrocellulose filters (Hybond, Amersham, Arlington Heights, IL). Specific protein bands were detected by the ECL detection method according to the manufacturer's instruction.

The α_{1A} subunits were detected using polyclonal antisera, whereas α_2 and β_{1b} subunits were visualized by monoclonal antibodies (supplied by W. Smith, Lilly Research Centre Limited, Erl Wood Manor, Windlesham, Surrey, UK).

Electrophysiology

Functional expression of recombinant Ca^{2+} channels in transfected cells was evaluated 48 h after transfection using the whole-cell patch clamp technique (Hamill et al., 1981). Transfected cells were identified by FDG staining (Molecular Probes, Inc., Eugene, OR) or with CD4 antibody-coated Dynabeads (Dynal, A.S., Oslo, Norway). Whole-cell currents were

recorded using an Axopatch-200A (Axon Instruments, Foster City, CA) or an EPC-9 (HEKA elektronik, Lambrecht, Germany) patch clamp amplifier, low-pass filtered at 1 kHz (−3 dB, 8-pole Bessel filter) and digitized at a rate of 10 kHz unless otherwise stated. For tail current measurements, electrodes were coated with Sylgard (Dow Corning, Midland, MI), supercharging was applied to reduce the expected charging time constant for the cells to <4 μs, and the digitization/filter rates were 50/16 kHz. Linear leak and residual capacitive currents were digitally on-line subtracted using a P/4 protocol. The holding potential was (V_h) −90 mV unless otherwise noted. Steady-state inactivation was determined from a holding potential of −100 mV by a test pulse to +10 mV (p1), followed by a 20-s prepulse from −100 mV to +20 mV in 10-mV decrements (pHold) preceding a second test pulse to +10 mV (p2). The digitization rate was 0.5 kHz during p1 and pHold and 2.5 kHz during p2. Pipettes were manufactured from TW150 glass (WPI, Sarasota, FL) and had resistance of 1.1–1.4 MΩ when filled with internal solution. Series resistance was 2–4 MΩ and 70–95% series resistance compensation was generally used. The pipette solution contained (in mM): 135 CsCl, 10 EGTA, 1 $MgCl_2$, 10 HEPES (pH 7.3, adjusted with TEA-OH). The external solution contained (in mM): 15 $BaCl_2$, 150 choline chloride, 5 TEA-Cl 1 $MgCl_2$, and 10 HEPES (pH 7.3, adjusted with TEA-OH). In studies where the external Ca^{2+} concentration was 15, 0.3, or 0 mM, the solution contained (in mM): 120 NaCl, 10 HEPES, and 15 or 0.3 $CaCl_2$ or 10 EGTA, respectively. All recordings were performed on single cells at room temperature (19–24°C). All values given as mean ± SD unless otherwise stated. Differences between the wt $\alpha_{1A\text{-}2}$ and mutant α_{1A} subunits in current magnitude (or fold increase) and inactivation kinetics were tested for statistical significance by an analysis of variance (ANOVA) followed by a post-hoc Dunnett's test (SigmaStat 1.01, Jandel Scientific). Statistical analysis revealed identical results for comparison of current amplitudes and fold increase, thus in the text only statistical values for fold increase are shown. All reagents were obtained from Sigma Chemical Co. (St. Louis, MO). The peptide toxin ω-Aga IVA was obtained from Pfizer Inc. (Groton, CT) and all ω-Aga IVA containing solutions also contained 1 mg/ml cytochrome *c*.

RESULTS

Cloning and functional expression of the human α_{1A} Ca^{2+} channel subunit

Overlapping cDNAs encoding the entire human neuronal α_{1A} subunit were isolated and sequenced. The translation initiation site was assigned to the first methionine that appears downstream of an in-frame nonsense codon (α_{1A} nt −120 to −118). The α_{1A} subunit shares the same predicted transmembrane topography as described previously for other Ca^{2+} channel α_1 subunits (Catterall et al., 1993). After characterizing human cDNAs we identified nucleotide alterations near the COO^--terminus that result in the expression of two α_{1A} isoforms, $\alpha_{1A\text{-}1}$ and $\alpha_{1A\text{-}2}$. The sequence of cDNAs encoding the $\alpha_{1A\text{-}2}$ variant contained a five-nucleotide (nt) deletion relative to $\alpha_{1A\text{-}1}$ ($\alpha_{1A\text{-}1}$ nt 6799 to 6803) that produces an in-frame nonsense codon immediately following the deletion, and results in a truncated COOH-terminus in the protein. These nucleotide alterations likely result from alternative RNA splicing. The human $\alpha_{1A\text{-}1}$ and $\alpha_{1A\text{-}2}$ variants encode for proteins containing 2510 and 2266 amino acids with a predicted molecular weight of 282,873 and 257,440, respectively. The α_{1A} sequences contain a 33-nt CAG repeat near the COO^- terminus that encodes 11 consecutive glutamine residues (Q) in the $\alpha_{1A\text{-}1}$ sequence. In $\alpha_{1A\text{-}2}$ the CAG repeat lies within the 3′ untranslated region as it occurs after the 5-nt deletion that results in the shorter COO^- terminus. The $\alpha_{1A\text{-}1}$ variant is 99.3% identical to the human isoform BI–1-GGCAG described by Zhuchenko et al. (1997) and is 92.1 and 91.3% identical to the rabbit BI-2 and rat rbA-1 isoforms (Mori et al., 1991; Starr et al., 1991). The $\alpha_{1A\text{-}2}$ variant is 99.5 and 99.1% identical to the human isoforms BI–1 and CACHL1A4 (Zhuchenko et al., 1997; Ophoff et al., 1996), has 94.8% identity to rabbit BI-1 (Mori et al., 1991), and 93.7% to rat rbA (Starr et al., 1991). Ophoff et al. (1996) did not describe the longer form of α_{1A} that corresponds to the human $\alpha_{1A\text{-}1}$ variant.

There are several important differences between the α_{1A} sequences described by Ophoff et al. (1996) and Zhuchenko et al. (1997) and the sequence reported here. First, the sequence described here contains insertions of amino acid(s) in the domain II-III linker (VEA at 726–728, E at 1204) and in the IVS3-S4 linker (NP at 1655–1656) that were not described by Ophoff et al. (1996) or Zhuchenko et al. (1997). Second, the sequence described here and that described by Zhuchenko et al. (1997) is identical at locations 899(D; II-III loop), 1462(G; IIIS5-S6 linker), 1607 (V), and 1620 (V; IVS2), but differs from that described by Ophoff et al. (1996) ($D^{899}\rightarrow G$, $G^{1462}\rightarrow A$, $V^{1607}\rightarrow A$, $V^{1620}\rightarrow A$). Third, at 10 locations within the COO-terminus the sequences described by Ophoff et al. (1996) and Zhuchenko et al. (1997) are identical but differ from those described here ($W^{1849}\rightarrow C$, $M^{1852}\rightarrow I$, $P^{1853}\rightarrow H$, $L^{1855}\rightarrow K$, $Q^{1859}\rightarrow S$, $M^{1860}\rightarrow L$, $H^{1863}\rightarrow V$, $M^{1864}\rightarrow I$, $A^{1876}\rightarrow H$, $Y^{1880}\rightarrow C$).

The identified α_{1A} sequence was confirmed by the isolation and characterization of multiple cDNA clones or PCR products from a single source. Based on the genomic sequence presented by Ophoff et al. (1996) the insertion of amino acid residues VEA in the II-III linker is likely due to the selection of alternate splice acceptor sites. Some of the differences in amino acid sequence determined in the three studies may represent additional splice variants of α_{1A} (see below).

We examined the biophysical properties of Ca^{2+} channels in HEK293 cells after transient transfection with cDNAs encoding human $\alpha_{1A\text{-}2}$, $\alpha_{2b}\delta$, and β_{1b} subunits. Currents recorded from cells in an external solution containing 15 mM Ba^{2+} as charge carrier were rapidly activating (Fig. 1 *A*) and slowly inactivating (Fig. 1 *B*). Peak inward currents were maximal at test potentials between +10 and +20 mV, and no inward current was observed at +80 mV (Fig. 1 *C*). Currents were also detected with Ca^{2+} channels containing the $\alpha_{1A\text{-}1}$ splice variant (data not shown), thus both splice variants we have isolated can be functionally expressed. In this study we have focused on characterization of the $\alpha_{1A\text{-}2}$ splice variant.

We investigated the voltage-dependence of activation and deactivation kinetics of $\alpha_{1A\text{-}2}\alpha_{2b}\delta\beta_{1b}$ Ca^{2+} channels. The time constant for the voltage-dependence of activation was determined by fitting a single exponential to the onset of the current trace. For membrane potentials between −20 and +10 mV the average value of the activation time constant

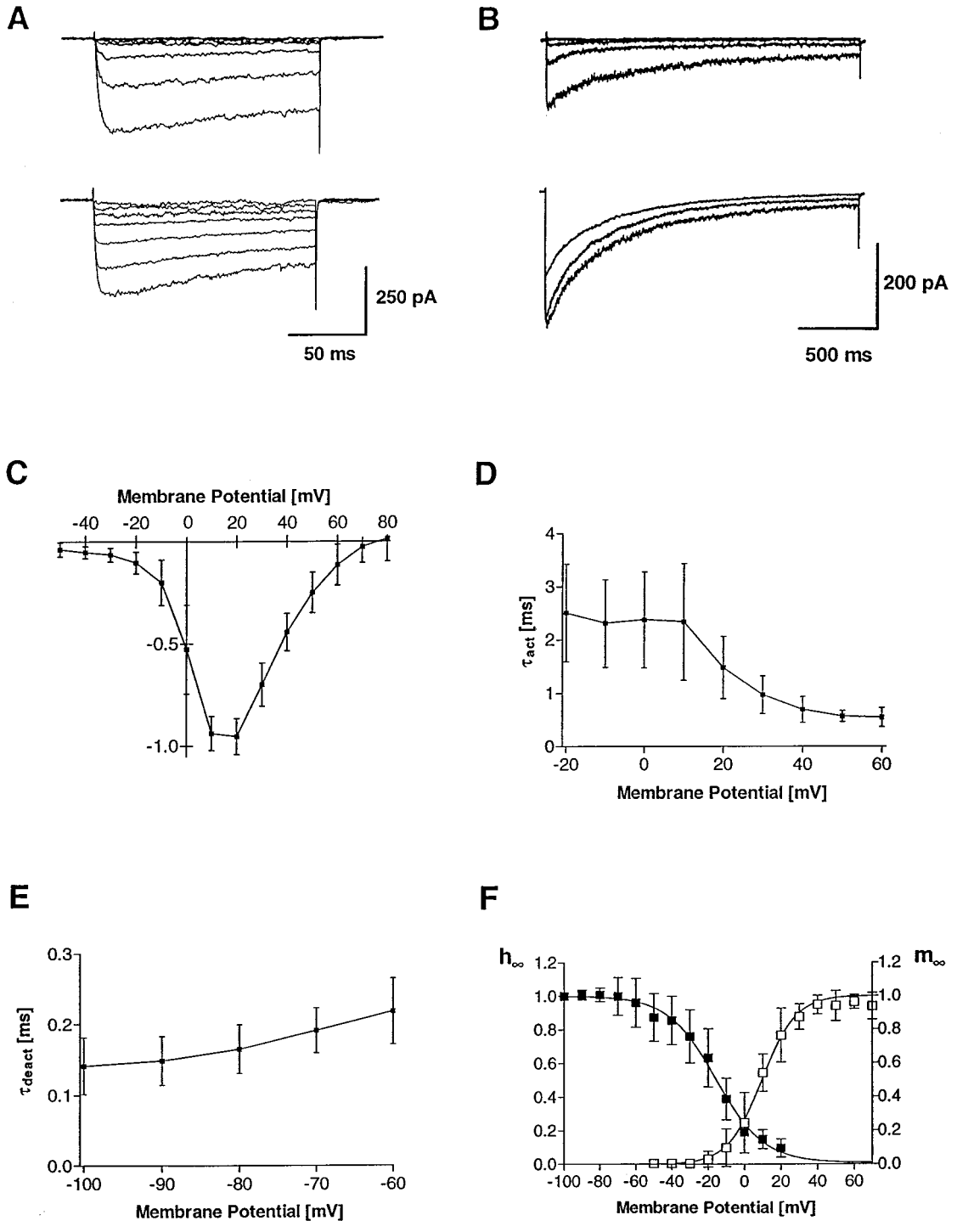

FIGURE 1 Biophysical properties of Ba^{2+} currents recorded from $\alpha_{1A\text{-}2}\alpha_{2b}\delta\beta_{1b}$ Ca^{2+} channels in HEK293 cells. (*A*) Examples of current traces elicited by 150-ms test pulses from a holding potential of −90 mV to between −50 mV and +10 mV, top panel, and between +20 mV and +80 mV, bottom panel. (*B*) Examples of current traces elicited by 2-s test pulses from a holding potential of −90 mV to between −30 mV and 0 mV, top panel, and between +10 mV and +30 mV, bottom panel. (*C*) Current-voltage relationship from traces, as in (*A*) normalized to the peak current in each cell and averaged. Points represent the mean ± SD ($n = 6$). (*D*) The time constant for kinetics of activation of I_{Ba} determined by fitting the rising phase of the current with a single exponential is plotted against the test potential. Data points represent the mean ± SD ($n = 5$). (*E*) Time constant for kinetics of deactivation determined by the single exponential fit of the tail current. Tail currents were elicited by repolarizations to voltages ranging from −100 to −60 mV after a brief depolarization to +60 mV. (*F*) Voltage-dependence of activation (m_∞) and isochronal inactivation (h_∞). The amplitude of tail currents was determined by extrapolating the tail current to the time of the end of the test pulse. Normalized tail current amplitudes were plotted (*open symbols*, mean ± SD) versus test potential. Data were fitted by a Boltzmann function $m_\infty = [1 + \exp(-(V_{test} - V_{1/2})/k)]^{-1}$, $V_{1/2} = +9.5$ mV, $k = 12.8$ mV, $n = 5$. Isochronal inactivation was determined from a holding potential of −100 mV by a test pulse to +10 mV (p1), followed by a 20-s prepulse from −100 mV to +20 mV in 10 mV decrements (pHold) preceding a second test pulse to +10 mV (p2). Normalized current amplitudes were plotted (*closed symbols*, mean ± SD) versus holding potential. Data were fitted by a Boltzmann function $h_\infty = [1 + \exp((V_{hold} - V_{1/2})/k)]^{-1}$, $V_{1/2} = -17$ mV, $k = 8.6$ mV, $n = 5$.

was 2.2 ms (at +10 mV: 2.17 ± 1.1 ms, $n = 8$) and it declined at more depolarized potentials (+20 to +60 mV), reaching 0.6 ms at +60 mV (Fig. 1 *D*). The voltage-dependence of deactivation kinetics was determined by tail-current analysis by fitting a single exponential to the decay of the tail current (Fig. 1 *E*). The average deactivation time constant at −90 mV was 148 ± 34 μs ($n = 6$) for the $\alpha_{1A\text{-}2}\alpha_{2b}\delta\beta_{1b}$ Ca^{2+} channel, a value similar to that reported for native and recombinant HVA Ca^{2+} channels (Matteson and Armstrong, 1986; Williams et al., 1994; Bleakman et al., 1995).

We further determined isochronal inactivation (h_∞) and steady-state activation (m_∞). Isochronal inactivation of $\alpha_{1A\text{-}2}\alpha_{2b}\delta\beta_{1b}$ Ca^{2+} channels (Fig. 1 *F*) was determined using a 20-s inactivating prepulse. The voltage-dependence of activation, or steady-state activation (m_∞), of $\alpha_{1A\text{-}2}\alpha_{2b}\delta\beta_{1b}$ Ca^{2+} channels was determined from tail currents elicited at different test potentials. The voltage for half-maximal inactivation ($V_{1/2}$) was −17 mV, ~30 mV less negative than human α_{1B} or α_{1E} recombinant HVA Ca^{2+} channels, and the $V_{1/2}$ for activation was +9.5 mV (Fig. 1 *F*), which is similar to other HVA Ca^{2+} channels (Williams et al., 1994; Bleakman et al., 1995).

Ca^{2+} channels containing $\alpha_{1A/B}$ chimeras

Transient transfection of the human $\alpha_{1A\text{-}2}$ or $\alpha_{1B\text{-}1}$ calcium channel subunits with the human $\alpha_{2b}\delta$ and β_{1b} subunits in HEK293 cells resulted in functional expression of Ca^{2+} channels with distinct biophysical properties. Cells expressing $\alpha_{1B\text{-}1}$-containing Ca^{2+} channels had robust voltage-activated Ba^{2+} currents (Fig. 2 *A*, 2712 ± 830 pA, $n = 25$), whereas currents from $\alpha_{1A\text{-}2}$-expressing cells were ~15-fold smaller (Fig. 2 *A*, 185 ± 161 pA, mean ± SD, $n = 73$). The current-voltage relationships for $\alpha_{1A\text{-}2}$- and $\alpha_{1B\text{-}1}$-containing Ca^{2+} channels were very similar with current thresholds at −40 mV, maximum current at +10 mV, and reversal of currents positive to +70 mV (Fig. 2 *A*). Both Ca^{2+} channels also have very similar activation kinetics ($\tau_{act(+10mV)}$ $\alpha_{1A\text{-}2}$: 2.17 ± 1.1 ms, $n = 8$; $\alpha_{1B\text{-}1}$: 2.31 ± 0.89 ms, $n = 5$) but differ markedly in their inactivation kinetics. The $\alpha_{1B\text{-}1}$-containing channel inactivates ~2-fold faster than the $\alpha_{1A\text{-}2}$-containing channel (Fig. 2 *B*, see below), and the two channels differ in their $V_{1/2}$ of isochronal inactivation by 42 mV (Fig. 1 *F*; Bleakman et al., 1995).

To determine whether discrete structural elements of the $\alpha_{1A\text{-}2}$ subunit are responsible for these differences in the current magnitude, a series of $\alpha_{1A/B}$ chimeras were constructed using an $\alpha_{1A\text{-}2}$ backbone and evaluated in transient expression experiments with the human $\alpha_{2b}\delta$ and β_{1b} subunits. Based upon recent studies suggesting that COO^--terminal sequences of the α_{1C} subunit influence Ca^{2+} channel current magnitude (Wei et al., 1994), construction of chimeras was initially focused on the COO^- terminus of $\alpha_{1A\text{-}2}$.

In the first α_1 chimera, designated $\alpha_{1A/B(a)}$, the COO^- terminus of the wt human $\alpha_{1A\text{-}2}$ subunit was replaced with the corresponding human wt $\alpha_{1B\text{-}1}$ sequence (Fig. 3 *A*). The

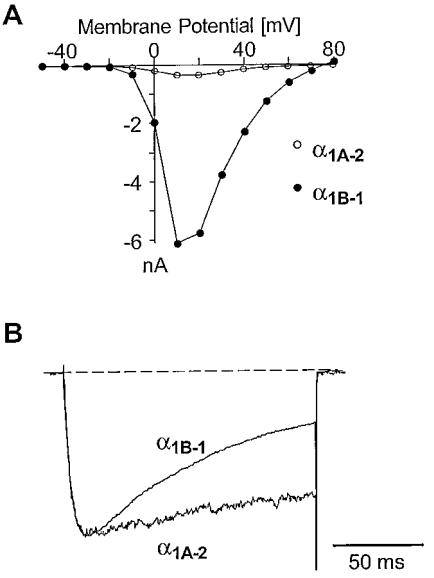

FIGURE 2 Comparison of the current-voltage and kinetic properties of $\alpha_{1A\text{-}2}\alpha_{2b}\delta\beta_{1b}$ and $\alpha_{1B\text{-}1}\alpha_{2b}\delta\beta_{1b}$ calcium channels expressed in HEK293 cells. (*A*) Average current-voltage relationships from cells expressing human $\alpha_{1A\text{-}2}\alpha_{2b}\delta\beta_{1b}$ and $\alpha_{1B\text{-}1}\alpha_{2b}\delta\beta_{1b}$ Ca^{2+} channels. Data points represent the mean ± SD ($n = 6$). (*B*) Normalized current traces illustrate similarities in activation kinetics and differences in inactivation kinetics for $\alpha_{1A\text{-}2}\alpha_{2b}\delta\beta_{1b}$ and $\alpha_{1B\text{-}1}\alpha_{2b}\delta\beta_{1b}$ Ca^{2+} channels. Currents were elicited by step depolarizations to +10 mV from a holding potential of −90 mV.

magnitude of Ba^{2+} current from cells expressing $\alpha_{1A/B(a)}$ was similar to that from cells expressing the wt $\alpha_{1A\text{-}2}$ subunit (Fig. 3 *B*, $n = 12$; $p > 0.3$), indicating that the $\alpha_{1A\text{-}2}$ COO^- terminus was not responsible for the differences in current magnitude. The second chimera, $\alpha_{1A/B(b)}$, contained $\alpha_{1B\text{-}1}$ sequence from IIIS6 to the COO^- terminus (Fig. 3 *A*). The current magnitude in cells expressing the $\alpha_{1A/B(b)}$ subunit was significantly larger (29.2 ± 17.2-fold, $n = 4$; $p < 0.05$) than in cells expressing the wt $\alpha_{1A\text{-}2}$ subunit (Fig. 3 *B*). These data suggested that amino acid sequences between IIIS6 and the COO^- terminus were critical for the observed increase in current magnitude, and $\alpha_{1A/B(c)}$ through $\alpha_{1A/B(f)}$ were constructed to localize the critical region. Substitution of α_{1B} sequence from IVS3 to the COO^- terminus ($\alpha_{1A/B(c)}$) also significantly increased current magnitude (10.1 ± 5.4-fold, $n = 4$; $p < 0.05$). In $\alpha_{1A/B(d)}$, narrowing the α_{1B} sequence to the IVS3 to IVS6 region resulted in a significant increase in current magnitude (23.6 ± 12.9-fold, $n = 4$; $p < 0.05$). Finally, the role of the putative pore-forming region in repeat IV was also investigated by construction of $\alpha_{1A/B(e)}$ and $\alpha_{1A/B(f)}$, each replacing approximately one-half of the $\alpha_{1A\text{-}2}$ pore-forming region with the corresponding $\alpha_{1B\text{-}1}$ sequence (Fig. 3 *B*). Replacement of the IVSS2 to IVS6 segment with $\alpha_{1B\text{-}1}$ sequence ($\alpha_{1A/B(e)}$) resulted in Ca^{2+} channels with current magnitudes similar to those containing wt $\alpha_{1A\text{-}2}$. In contrast, replacement of the $\alpha_{1A\text{-}2}$ IVS3 to the end of the IVSS1 segment with the corresponding $\alpha_{1B\text{-}1}$ sequence ($\alpha_{1A/B(f)}$) resulted in a significant increase in current magnitude (28.3 ± 25.1-fold, $n = 14$; $p < 0.05$; Fig. 3 *B*).

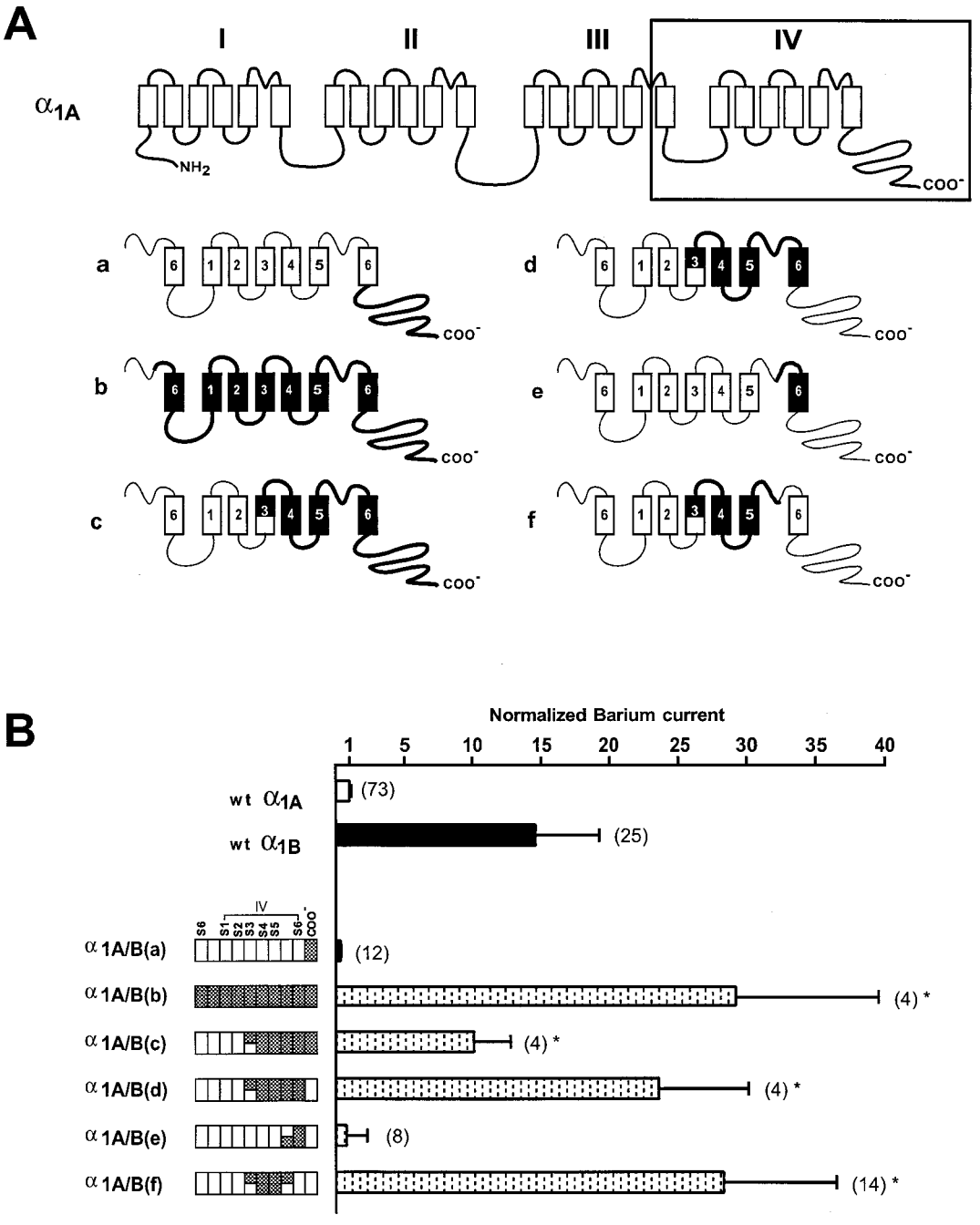

FIGURE 3 Chimeras of human α_{1A-2} and α_{1B-1} Ca^{2+} channel subunits. (*A*) The predicted transmembrane topography of the α_1 subunit of voltage-dependent calcium channels. Human α_{1A}/α_{1B} chimeras were constructed by substituting various segments of α_{1B} sequence within the corresponding COO^- region of the α_{1A} subunit (*boxed region*). (*A*) (*a–f*): Models of $\alpha_{1A/B(a)}$-$\alpha_{1A/B(f)}$; the thin lines and open boxes represent α_{1A} sequences and the heavy lines and filled boxes represent α_{1B} sequence. (*B*) Comparison of maximum inward current magnitude for recombinant Ca^{2+} channels containing $\alpha_{2b}\delta\beta_{1b}$ with α_{1A-2}, α_{1B-1}, or $\alpha_{1A/B(a)}$-$\alpha_{1A/B(f)}$. Maximum inward barium currents were normalized with respect to that of the $\alpha_{1A-2}\alpha_{2b}\beta_{1b}$ Ca^{2+} channel. Data points represent mean + SD and the *n* values for the individual experiment are given in parentheses above the bar. ∗, values significantly different from control ($\alpha_{1A-2}\alpha_{2b}\beta_{1b}$) at $p < 0.05$. Shaded boxes at left represent α_{1B} sequence, whereas open boxes represent α_{1A} sequence.

Identification of amino acids in domain IV of the α_{1A} subunit involved in the control of biophysical properties

These results limited the critical region responsible for increasing current magnitude to the IVS3 to IVSS2 region encompassing a region of 112 amino acids (Fig. 4 *A*). There are 20 amino acid differences between α_{1A-2} and α_{1B-1} subunits within this region and all of these are located in putative extracellular loops. Based on a comparison of α_{1A-2} with other classes of known human neuronal α_1 sequences (Fig. 4 *A*), 13 of these 20 amino acids with nonconservative changes could be further subdivided into three groups that might be responsible for the effects observed in the chime-

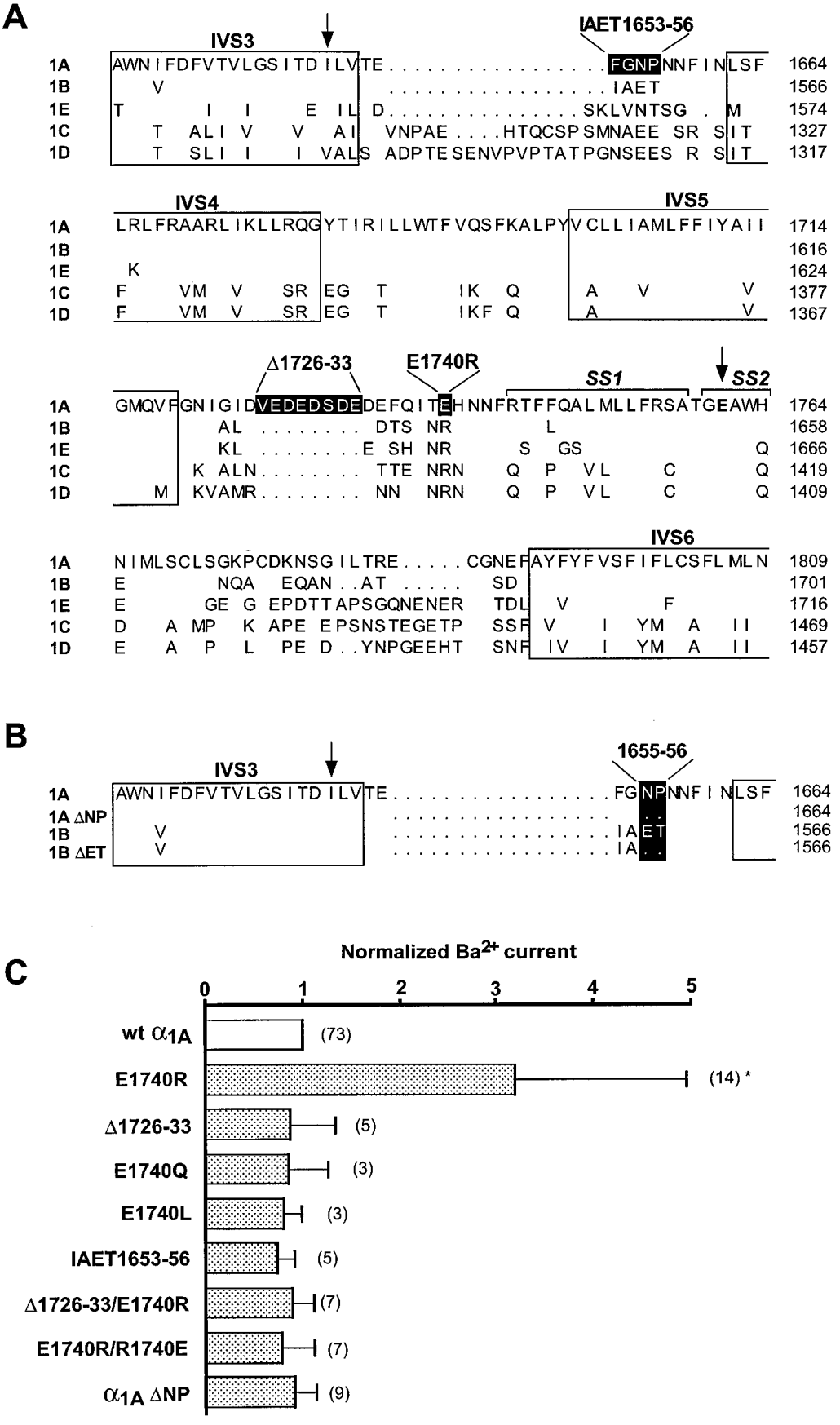
A
IVS3
IAET1653-56
1A AWNIFDFVTVLGSITDILVTE . . . . . FGNPNNFINLSF 1664
1B V . . . . . IAET 1566
1E T I I E IL D . . . . . SKLVNTSG . M 1574
1C T ALI V V AI VNPAE . . . . HTQCSP SMNAEE SR SIT 1327
1D T SLI I I VALS ADPTE SENVPVPTATPGNSEES R SIT 1317
IVS4
IVS5
1A LRLFRAARLIKLLRQGYTIRILLWTFVQSFKALPYVCLLIAMLFFIYAII 1714
1B 1616
1E K 1624
1C F VM V SR EG T IK Q A V V 1377
1D F VM V SR EG T IKF Q A V 1367
Δ1726-33
E1740R
SS1
SS2
1A GMQVFGNIGIDVEDEDSDEDEFQITEHNNFRTFFQALMLLFRSATGEAWH 1764
1B AL . . . . . DTS NR L 1658
1E KL . . . . . E SH NR S GS Q 1666
1C K ALN . . . . . TTE NRN Q P VL C Q 1419
1D M KVAMR . . . . . NN NRN Q P VL C Q 1409
IVS6
1A NIMLSCLSGKPCDKNSGILTRE . . . . . CGNEFAYFYFVSFIFLCSFLMLN 1809
1B E NQA EQAN . . AT . . . . . SD 1701
1E E GE G EPDTTAPSGQNENER TDL V F 1716
1C D A MP K APE EPSNSTEGETP SSF V I YM A II 1469
1D E A P L PE D . . YNPGEEHT SNF IV I YM A II 1457
B
1655-56
IVS3
1A AWNIFDFVTVLGSITDILVTE . . . . . FGNPNNFINLSF 1664
1A ΔNP 1664
1B V . . . . . IAET 1566
1B ΔET V . . . . . IA . . 1566
C
Normalized Ba2+ current
0 1 2 3 4 5
wt α1A (73)
E1740R (14) *
Δ1726-33 (5)
E1740Q (3)
E1740L (3)
IAET1653-56 (5)
Δ1726-33/E1740R (7)
E1740R/R1740E (7)
α1A ΔNP (9)

ras: 1) a cluster of four contiguous amino acids located within the extracellular linker between IVS3 and IVS4 which included changes in size and charge, 2) an additional eight contiguous amino acids in the extracellular loop linking IVS5 and IVSS1, which adds six negative charges and length to the IVS5-IVS6 linker, and 3) a glutamate residue at position 1740, also in the putative IVS5-IVSS1 extracellular loop (Fig. 4 *A*). The negatively charged glutamate at position 1740 is unique to α_{1A} subunits; all other α_1 subunits have a positively charged arginine at the equivalent position. Interestingly, the glutamate at position 1740 is conserved among all cloned α_{1A} subunits (rat, rabbit, and human) whereas all other cloned α_1 subunits (α_{1B}–α_{1E} and α_{1S}) have an arginine at the corresponding position (rat, rabbit, human, ray, mouse, hamster, *Drosophila*, and carp). To limit the number of mutations, we altered each of the three amino acid groupings in the wt α_{1A-2} subunit individually by site-directed mutagenesis to the corresponding α_{1B-1} sequence. The resulting three constructs are designated α_{1A}IAET1653-56, deletion $\alpha_{1A}\Delta$1726-33, and the single-point mutation α_{1A}E1740R (Fig. 4 *A*). The other seven amino acid differences in this region between α_{1A} and α_{1B} that were considered conservative changes were not addressed in this study.

Transient expression experiments with α_{1A}IAET1652-56 or $\alpha_{1A}\Delta$1726-33 resulted in functional calcium channels, but neither construct enhanced the current magnitude to the level of the wt α_{1A-2}-containing Ca^{2+} channel (Fig. 4 *C*). In contrast, exchange of the negatively charged glutamate for the positively charged arginine at position 1740 (E1740R) of the α_{1A-2} subunit significantly enhanced the current magnitude (3.2 ± 1.75-fold, $n = 14$; $p < 0.05$) compared to results with wt α_{1A-2}. The specificity of the enhancement observed with the α_{1A}E1740R mutation is shown by the reverse mutation α_{1A}E1740R/R1740E, which restored the current magnitude to that of the wt α_{1A-2}-containing Ca^{2+} channel. Exchange of glutamate for the neutral amino acids glutamine (α_{1A}E1740Q) or alanine (α_{1A}E1740L) had no detectable effect on current magnitude (Fig. 4 *C*). Interestingly, introduction of the mutation analogous to α_{1A}E1740R in the α_{1B-1} subunit (R1634E), followed by transient coexpression with the $\alpha_{2b}\delta$ and β_{1b} subunits, resulted in Ca^{2+} channels with current magnitudes and kinetics similar to cells expressing the wt α_{1B-1} subunit (1.0 ± 0.4-fold increase, $n = 4$; data not shown). These experiments demonstrate that an arginine residue in the IVS5-IVS6 linker is important for current enhancement in Ca^{2+} channels containing the α_{1A-2} but not the α_{1B-1} subunit.

The IVS3-SS1 region in the human α_{1A} clone that seems critical for current enhancement has two additional amino acids ($N^{1655}P^{1656}$) that are not found in rabbit, mouse, or the two recently described human α_{1A} clones (Mori et al., 1991; Fletcher et al., 1996; Zhuchenko et al., 1997; Ophoff et al., 1996). To test whether deletion of $N^{1655}P^{1656}$ could produce enhancement in current magnitude similar to $\alpha_{1A/B(f)}$ we constructed the deletion mutant $\alpha_{1A}\Delta$NP (Fig. 4 *B*). Transient expression of $\alpha_{1A}\Delta$NP resulted in functional calcium channels with current magnitude similar to that of wt α_{1A-2}-containing Ca^{2+} channels (Fig. 4 *C*), but with significantly altered biophysical and pharmacological properties (see below).

Expression of polypeptides representing chimera $\alpha_{1A/B(f)}$ and mutation α_{1A}E1740R

To determine whether the increase in current magnitude observed with $\alpha_{1A/B(f)}$- or α_{1A}E1740R-containing Ca^{2+} channels resulted from an increase in the levels of Ca^{2+} channel subunit proteins in the cell membrane, we used immunoblot analysis to compare the levels of protein expression of the α_1, $\alpha_{2b}\delta$, and β_{1b} subunits. Subunits were detected by immunostaining with polyclonal antisera specific to the α_{1A} subunit or monoclonal antibodies specific to the $\alpha_2\delta$ and β_{1b} subunits (Fig. 5 *A*). Although there was no detectable α_{1A} or β_{1b} protein in untransfected HEK293 cells, there appeared to be a very low level of $\alpha_2\delta$ protein expressed in these cells (Fig. 5 *A*). The protein levels of the α_1 and the β_{1b} subunits were moderately elevated in cells expressing the α_{1A}E1740R subunit compared to those expressing wt α_{1A-2}, averaging increases of ~2.1- and 2.0-fold, respectively, as determined by densitometric analysis of the immunoblot (Fig. 5 *B*). A more substantial increase in protein level was observed in cells expressing $\alpha_{1A/B(f)}$,

FIGURE 4 Involvement of amino acid residues in the IVS3 to IVS6 region of the human Ca^{2+} channel α_{1A-2} subunits in determining current amplitude. (*A*) An alignment of the human neuronal α_{1A}-α_{1E} subunit amino acid sequences through the IVS3-IVS6 transmembrane segments showing only those residues in α_{1B}-α_{1E} that differ from α_{1A}. Dots represent gaps introduced to optimize the alignment. Putative transmembrane segments are enclosed in boxes and the putative pore-lining SS1/SS2 region is indicated by brackets above. $\alpha_{1A/B(f)}$ contains a substitution of amino acids 1648 to 1761 in α_{1A} (indicated by the two arrows) with the corresponding region of the α_{1B} subunit. Three points of nonconservative difference were identified between α_{1A} and α_{1B} in this 112-amino acid region and were, therefore, targeted for in vitro mutagenesis: α_{1A} $F_{1653}GNP_{1656}$ (IAET1653-56), $V_{1726}EDEDSDE_{1733}$ (Δ1726-33), and E_{1740} (E1740R). These amino acids are enclosed in shaded boxes in the α_{1A-2} sequence. All amino acids are located within putative extracellular loops. (*B*) Comparison of the IVS3-S4 spanning region for various neuronal α_{1A} and α_{1B} sequence. Dark shading represents the positions of residues that when absent in α_{1A} or α_{1B} subunits alter kinetic properties, and in α_{1A} ω-Aga IVA affinity. $\alpha_{1A}\Delta$NP corresponds to neuronal α_{1A} variants found in human, rat, and rabbit (Zhuchenko et al., 1997; Ophoff et al., 1996; Starr et al., 1991; Mori et al., 1991). $\alpha_{1B}\Delta$ET corresponds to neuronal α_{1B} variant found in rat and rabbit (Lin et al., 1997; Fujita et al., 1993; Dubel et al., 1992, 1994). (*C*) Comparison of maximum inward current magnitude for recombinant Ca^{2+} channels containing $\alpha_{2b}\delta$, β_{1b}, and either wt α_{1A-2}, α_{1A}E1740R, $\alpha_{1A}\Delta$1726-33, α_{1A}E1740Q, α_{1A}E1740L, α_{1A}IAET1653-56, $\alpha_{1A}\Delta$1726-33/E1740R, or α_{1A}E1740R/R1740E. Maximum inward barium currents were normalized with respect to that of the $\alpha_{1A-2}\alpha_{2b}\delta\beta_{1b}$ Ca^{2+} channel. Data points represent mean + SD and the n values for the individual experiment are given in parentheses above the bar. *, values are significantly different at $p < 0.05$ compared to the $\alpha_{1A-2}\alpha_{2b}\delta\beta_{1b}$ Ca^{2+} channel.

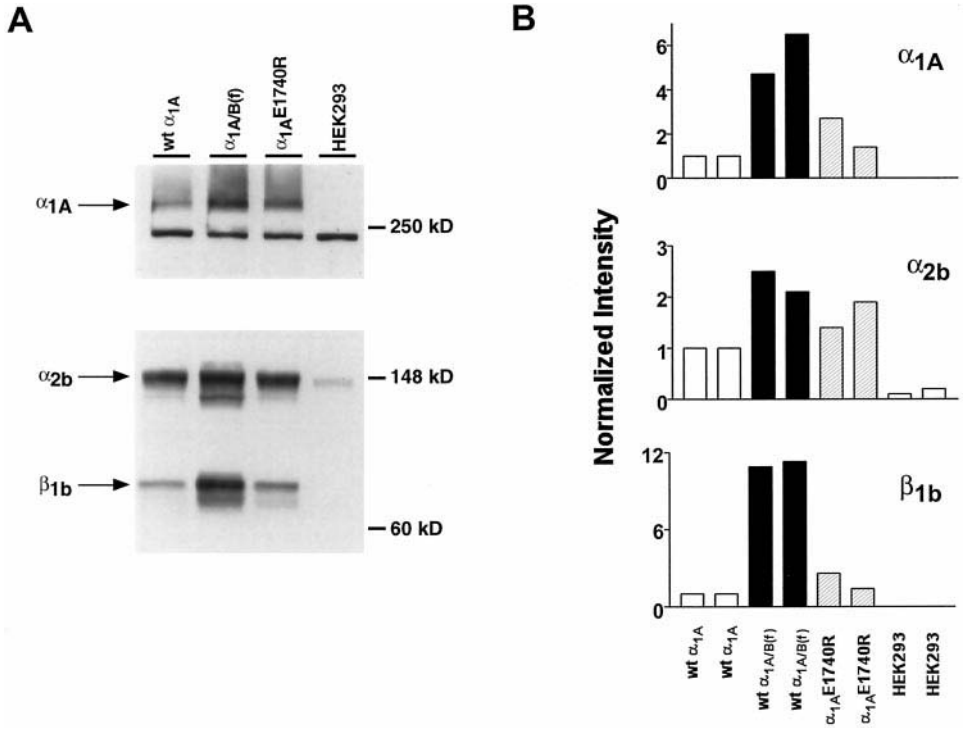

FIGURE 5 Immunoblot analysis of the expression of recombinant Ca^{2+} channel subunit polypeptides. (*A*) Immunoblot analysis of Ca^{2+} channel subunit polypeptides levels in membranes isolated from HEK293 cells transiently transfected with cDNAs encoding human $\alpha_{2b}\delta$ and β_{1b} together with $\alpha_{1A\text{-}2}$, $\alpha_{1A/B(f)}$, α_{1A}E1740R subunits or from untransfected cells. The different α_1 subunits are indicated above each lane. Filters were cut horizontally above the 148 kDa marker to allow identification of all three subunits on the same gel. Membrane proteins (30 μg per lane) were immunostained with affinity-purified α_{1A} polyclonal antisera (*top panel*) or monoclonal antibodies (mAb) specific for the $\alpha_2\delta$ or β_{1b} subunits (*bottom panel*). Since the polypeptides were separated under reducing conditions the α_{2b} subunit was dissociated from the δ subunit. Previous experiments indicate that the mAb for $\alpha_2\delta$ and β_{1b} do not cross-react (data not shown). The Ca^{2+} channel subunits are denoted with arrows. Quantitative analysis of expression levels of specific Ca^{2+} channels subunits is illustrated in (*B*). Values represent the amount of membrane protein obtained from total membranes in two separate sets of transfections. The data were normalized with respect to those obtained in the wt $\alpha_{1A\text{-}2}$ transfection. All transfection efficiencies were approximately equivalent (~50–60%) as determined by X-gal staining.

where the average increase was 5-fold for the $\alpha_{1A/B(f)}$ subunit and 11-fold for the β_{1b} subunit. The protein levels of the $\alpha_{2b}\delta$ subunit in cells transfected with α_{1A}E1740R or $\alpha_{1A/B(f)}$ increased only slightly, exhibiting 1.6- and 2.3-fold increases, respectively (Fig. 5 *B*). Thus, the increase in steady-state protein levels of the α_1, $\alpha_{2b}\delta$, and β_{1b} subunits within the membranes of cells expressing $\alpha_{1A/B(f)}$ or α_{1A}E1740R appears to correlate with the observed increase in current magnitude; however, it seems unlikely that changes in the biophysical properties (see below) of Ca^{2+} channels containing $\alpha_{1A/B(f)}$ or α_{1A}E1740R described below can be entirely attributable to these increases.

Biophysical properties of $\alpha_{1A/B(f)}$, α_{1A}E1740R, and $\alpha_{1A}\Delta$NP

To further understand the effects of $\alpha_{1A/B(f)}$, α_{1A}E1740R, and $\alpha_{1A}\Delta$NP mutant subunits on Ca^{2+} channel function, the biophysical properties of Ca^{2+} channels containing these subunits were examined in more detail. Fig. 6, *A–C* illustrates representative Ba^{2+} currents and the resulting current-voltage relationship of cells transiently expressing Ca^{2+} channels containing the α_{1A}E1740R or $\alpha_{1A}\Delta$NP subunit. Inward currents were elicited at potentials >-30 mV, peaked at $\sim+10$ mV, and reversed at potentials positive to $+80$ mV. The current-voltage relationships for Ca^{2+} channels containing $\alpha_{1A/B(f)}$ (data not shown) were very similar to those for channels containing wt $\alpha_{1A\text{-}2}$ or $\alpha_{1B\text{-}1}$ subunits (see Fig. 2 *A*).

In contrast to the current-voltage properties, the activation and the inactivation kinetics of channels containing $\alpha_{1A/B(f)}$, α_{1A}E1740R, and $\alpha_{1A}\Delta$NP subunits differed substantially from those containing wt $\alpha_{1A\text{-}2}$. The Ba^{2+} currents recorded from channels containing $\alpha_{1A/B(f)}$ or $\alpha_{1A}\Delta$NP activated faster than those from channels containing the wt $\alpha_{1A\text{-}2}$ subunit ($\tau_{act,+10\ mV}$; $\alpha_{1A/B(f)}$: 1.49 $\pm$ 0.4 ms, $p = 0.07$; $\alpha_{1A}\Delta$NP: 1.24 $\pm$ 0.48 ms, $p < 0.05$; wt $\alpha_{1A\text{-}2}$: 2.17 $\pm$ 1.1 ms; $n = 10$, 7, and 8, respectively; Fig. 6 *D*), whereas currents from channels containing α_{1A}E1740R had activation kinetics identical to the wt $\alpha_{1A\text{-}2}$ (2.1 $\pm$ 0.26 ms; $n = 8$; $p > 0.15$; Fig. 6 *D*). Similar results were also observed at different test potentials between -10 and $+40$ mV (data not shown). The time course of inactivation was also altered with $\alpha_{1A/B(f)}$, α_{1A}E1740R, and $\alpha_{1A}\Delta$NP compared to wt α_{1A} (Fig. 6 *D*) and the rate of inactivation was evaluated during 2-s depolarizations (Fig. 7). Inactivation kinetics were more

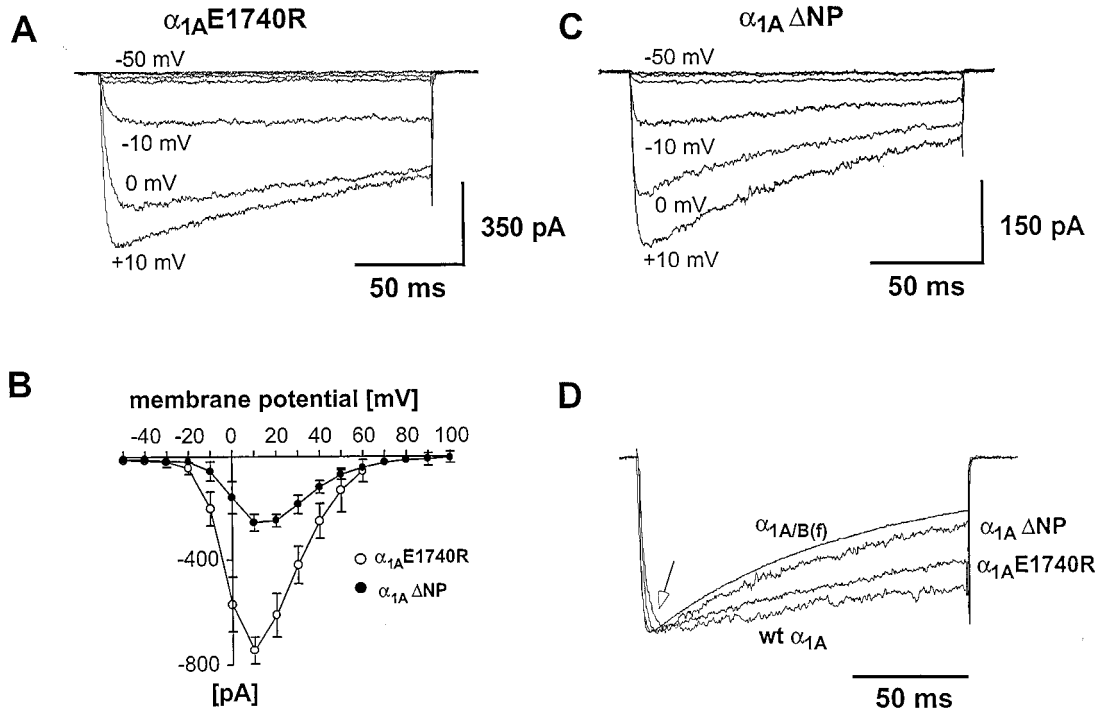

FIGURE 6 Mutants α_{1A}E1740R or $\alpha_{1A}\Delta$NP alter the kinetic properties of Ca^{2+} channels. (*A*, *C*) Examples of current traces from α_{1A}E1740R$\alpha_{2b}\delta\beta_{1b}$ or $\alpha_{1A}\Delta$NP$\alpha_{2b}\delta\beta_{1b}$ Ca^{2+} channels transiently expressed in HEK293 cells to test potentials between −50 and +10 mV in 10-mV increments. (*B*) The voltage-dependence of channel activation is similar for α_{1A}E1740R or $\alpha_{1A}\Delta$NP-containing channels, but the current magnitude is significantly increased with α_{1A}E1740R. Current-voltage relationships for α_{1A}E1740R and $\alpha_{1A}\Delta$NP were constructed from 12 and 9 cells, respectively. Data points represent mean ± SE. (*D*) Comparison of activation and inactivation kinetics of Ca^{2+} channels containing $\alpha_{1A/B(f)}$, α_{1A}E1740R, or $\alpha_{1A}\Delta$NP with those containing wt $\alpha_{1A\text{-}2}$. The rates of activation and inactivation are significantly increased for $\alpha_{1A/B(f)}$ and $\alpha_{1A}\Delta$NP compared to wt $\alpha_{1A\text{-}2}$ currents (*open arrow*) and are only marginally different for α_{1A}E1740R. Currents were elicited by step depolarizations to +10 mV from a holding potential of −90 mV. For comparison, traces were normalized and superimposed.

rapid in $\alpha_{1B\text{-}1}$- than $\alpha_{1A\text{-}2}$-containing Ca^{2+} channels (Fig. 7 *A*) and in both cases were best fit with the sum of two exponential functions. The time constant for the fast component (τ_1) was 2-fold faster for $\alpha_{1B\text{-}1}$ compared to wt $\alpha_{1A\text{-}2}$-containing Ca^{2+} channels (89 ± 13 vs. 179 ± 36 ms, $p < 0.001$, $n = 12$) while the time constant for the slow component (τ_2) was similar (see Table 1). The inactivation kinetics for α_{1A}E1740R-containing channels were qualitatively similar to those of channels containing wt $\alpha_{1A\text{-}2}$ (Fig. 7 *B*), but were best fit by a single exponential function. In contrast, the inactivation of $\alpha_{1A}\Delta$NP was similar to that of channels containing the wt $\alpha_{1B\text{-}1}$ subunit (Fig. 7 *C*, Table 1). The rate of inactivation was even further increased in $\alpha_{1A/B(f)}$-containing channels, which contains both mutations (Fig. 7 *D*). Similar differences in inactivation kinetics were observed for test potentials between 0 and +40 mV (data not shown). The faster rate of inactivation observed with α_{1B} or $\alpha_{1A/B(f)}$ is most likely a voltage-dependent rather than a calcium-dependent process, as there is no correlation between rate of inactivation and current magnitude in the range from 2 to 18 nA. ($r^2 = 0.05$, V_{test} 0–+30 mV, $n = 10$). These results indicate that amino acids $N^{1655}P^{1656}$ are important in determining the activation and inactivation kinetics of the channel. The further increase in rate of inactivation with $\alpha_{1A/B(f)}$ indicates that additional amino acids within the IVS3-S4 and/or the IVS5-SS1 linker are important in determining inactivation kinetics.

Ca^{2+} channels containing $\alpha_{1A/B(f)}$, α_{1A}E1740R, or $\alpha_{1A}\Delta$NP also displayed altered isochronal inactivation properties compared to those containing the wt $\alpha_{1A\text{-}2}$ subunit. Using a 20-s conditioning pulse, the $V_{1/2}$ of inactivation for $\alpha_{1A\text{-}2}$- and $\alpha_{1B\text{-}1}$-containing channels was −17 mV and −59 mV, respectively (Fig. 8 *A*). Ca^{2+} channels containing α_{1A}E1740R or $\alpha_{1A}\Delta$NP had a $V_{1/2}$ of −27 or −37 mV, respectively, corresponding to a shift of −10 or −20 mV compared to those containing the wt $\alpha_{1A\text{-}2}$ subunit. The $V_{1/2}$ value for channels containing $\alpha_{1A/B(f)}$ was −42 mV, a value much closer to the $V_{1/2}$ of $\alpha_{1B\text{-}1}$- than $\alpha_{1A\text{-}2}$-containing channels. Since we only examined this inactivation parameter with 20-s conditioning pulses, which might not be not long enough to reach true steady-state inactivation, it is possible that the observed differences in the $V_{1/2}$ values may reflect changes in the rate of inactivation rather than changes in the $V_{1/2}$ for steady-state inactivation.

It has been reported that four conserved glutamate residues, located at homologous positions in the putative pore-lining region (P-region) of each repeat of the α_1 subunit, are molecular determinants for ion selectivity and ion permeation of voltage-gated Ca^{2+} channels (Yang et al., 1993; Tang et al., 1993; Kim et al., 1993). The effect of the amino

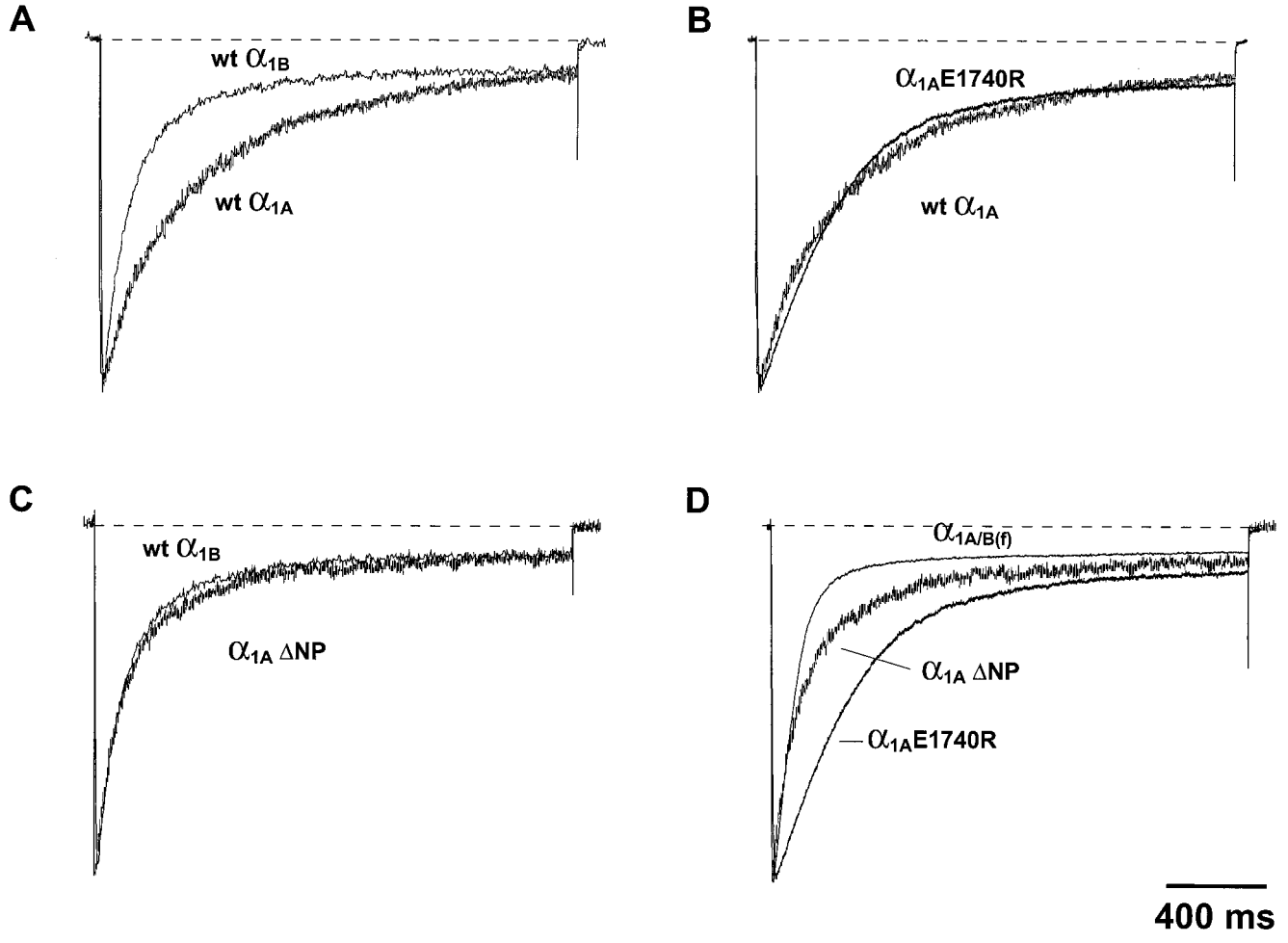

FIGURE 7 Comparison of inactivation kinetics of Ca^{2+} channels containing $\alpha_{1A\text{-}2}$, $\alpha_{1B\text{-}1}$, $\alpha_{1A/B(f)}$, or mutant α_{1A}E1740R. (*A–D*) Currents were recorded from HEK293 cells transiently expressing $\alpha_{2b}\delta\beta_{1b}$ and $\alpha_{1A\text{-}2}$, $\alpha_{1B\text{-}1}$, $\alpha_{1A/B(f)}$, α_{1A}E1740R, or $\alpha_{1A}\Delta$NP. All traces, except for α_{1A}E1740R, were fitted to a biexponential function of the form $I = A_0 + A_1 \exp(-t/\tau_1) + A_2 \exp(-t/\tau_2)$. The values for τ_1 and τ_2 are indicated in Table 1. Holding potential: −90 mV.

acid substitutions on ion selectivity outside the P-region, in the $\alpha_{1A/B(f)}$ or α_{1A}E1740R subunits, were evaluated. The interaction of Ca^{2+} ions with the mutant Ca^{2+} channels was assessed by examining the Ca^{2+} block of inward Na^+ current. Fig. 8 *B* illustrates current-voltage relationships of Ca^{2+} and Na^+ currents from channels containing the $\alpha_{1A/B(f)}$. In the absence of external Ca^{2+} (120 mM Na^+) the current magnitude increased by ~1.8-fold and the reversal potential (E_{rev}) shifted from +62 mV in the presence of Ca^{2+} (15 mM Ca^{2+}, 120 mM Na^+) to −2 mV. A similar shift in E_{rev} has been observed with channels containing the rabbit α_{1C} subunit expressed in *Xenopus* oocytes (Yang et al., 1993). The inward Na^+ current was reduced by 98% in the presence of 300 μM Ca^{2+} without shifting E_{rev}, indicating the block of the Na^+ current in the presence of micromolar concentrations of Ca^{2+} (Fig. 8 *B, inset*). Similar results were observed with channels containing the α_{1A}E1740R subunit (data not shown), suggesting that this mutation does not alter permeation properties.

ω-Aga IVA inhibits $\alpha_{1A}\Delta$NP more effectively than wt α_{1A}

Finally, we also examined the effects of ω-Aga IVA on Ca^{2+} channels containing wt $\alpha_{1A\text{-}2}$, $\alpha_{1A/B(f)}$, α_{1A}E1740R, or

TABLE 1 Comparison of inactivation kinetics of wt α_{1A}, wt α_{1B}, $\alpha_{1A/B(f)}$, or α_{1A} E1740R containing Ca^{2+} channels

	wt α_{1A}	wt α_{1B}	$\alpha_{1A/B(f)}$	α_{1A} ΔNP	E1740R
τ_1	179 ± 36 ms	89 ± 13 ms	78 ± 25 ms	81 ± 27 ms	347 ± 207 ms
A_1	62 ± 18%	66 ± 8%	72 ± 14%	46 ± 18%	69 ± 12%
τ_2	647 ± 59 ms	508 ± 220 ms	639 ± 336 ms	418 ± 119 ms	—
A_2	14 ± 16%	26 ± 4%	22 ± 6%	41 ± 19%	—

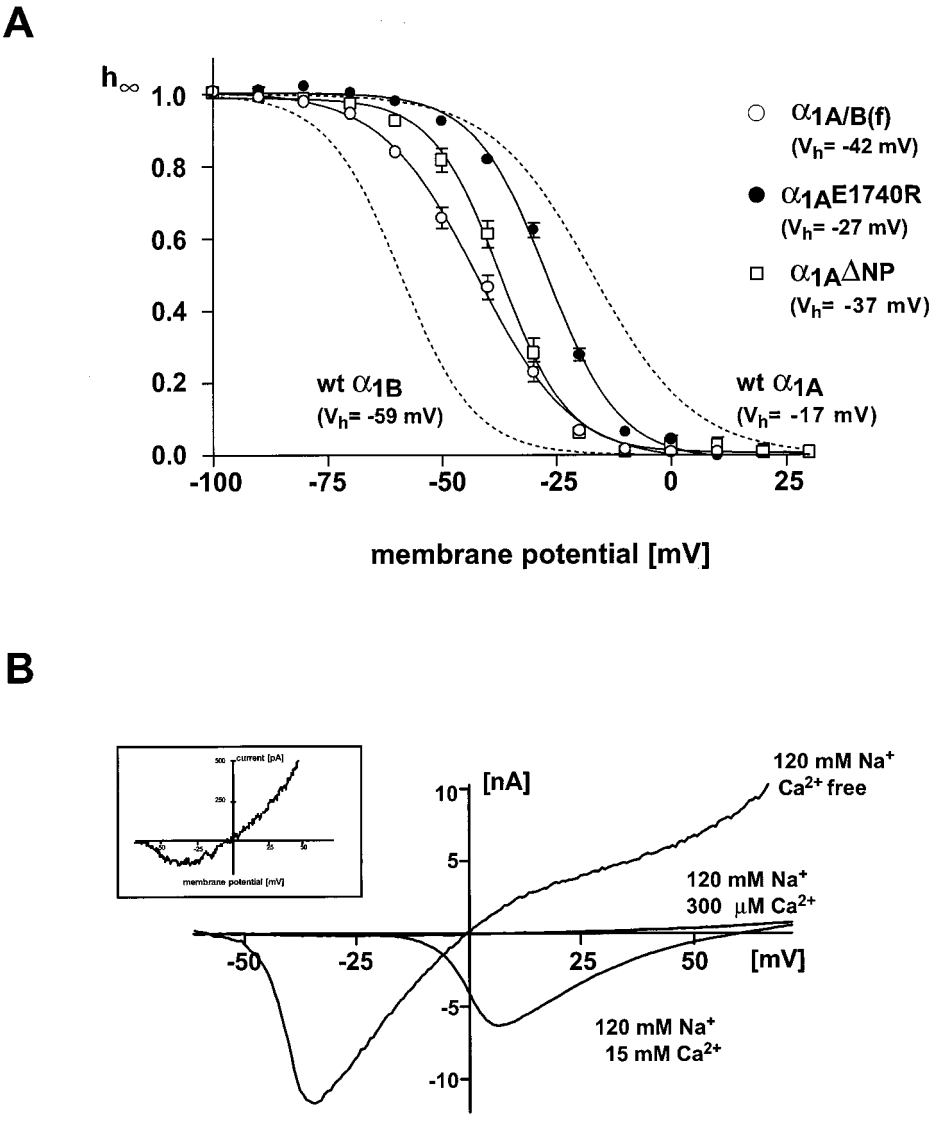

FIGURE 8 Isochronal inactivation (h_∞) of Ca^{2+} channels containing $\alpha_{1A\text{-}2}$, $\alpha_{1B\text{-}1}$, $\alpha_{1A/B(f)}$, α_{1A}E1740R, or $\alpha_{1A}\Delta$NP. (*A*) Isochronal inactivation was expressed as the ratio of two test pulses to +10 mV, separated by a 20-s inactivation pulse to membrane potentials between −100 and +10 mV. Note the 10 mV hyperpolarizing shift in steady-state inactivation with α_{1A}E1740R, the 20 mV with $\alpha_{1A}\Delta$NP, and the 30 mV shift with $\alpha_{1A/B(f)}$ compared to the wt $\alpha_{1A\text{-}2}$. Data were fitted by a Boltzmann function $h_\infty = [1 + \exp(V - V_{1/2})/k]^{-1}$ and best fits are shown as continuous lines for $\alpha_{1A/B(f)}$, E1740R, and $\alpha_{1A}\Delta$NP, and as dashed lines for wt $\alpha_{1A\text{-}2}$ (see also Fig. 1 *F* for original data) and $\alpha_{1B\text{-}1}$ (see Fig. 4, Bleakman et al., 1995 for original data). Values for $V_{1/2}/k$ are −59 mV/8.1 ($\alpha_{1B\text{-}1}$), −42 mV/10.2 ($\alpha_{1A/B(f)}$), −37 mV/7.3 ($\alpha_{1A}\Delta$NP), −27 mV/7.6 (α_{1A}E1740R), and −17 mV/11 ($\alpha_{1A\text{-}2}$). Data points represent mean ± SE, $n = 6$ for all experiments. Holding potential was −100 mV. (*B*) Inhibition of Na^+ currents through Ca^{2+} channels containing $\alpha_{1A/B(f)}$ by low concentrations of external Ca^{2+}. The current-voltage relationship for $\alpha_{1A/B(f)}$ was obtained with voltage-ramp protocol (−100 to +80 mV in 300 ms). The inset shows an enlarged scale of the current-voltage relationship obtained with 120 mM Na^+ + 300 μM Ca^{2+} in the external medium.

$\alpha_{1A}\Delta$NP, since α_{1A}-containing Ca^{2+} channels are sensitive to block by this peptide toxin. At a concentration of 1 μM, ω-Aga IVA inhibited currents from $\alpha_{1A\text{-}2}$- or α_{1A}E1740R-containing channels to a similar degree and showed a similar time course for the onset of block (54.6 ± 12.6% and 61.9 ± 16.9%; τ_{on}: 254 ± 44 and 204 ± 26 ms; Fig. 9, *B–D*). In contrast, the inhibition of $\alpha_{1A}\Delta$NP-containing channels was substantially faster and more complete (88.2 ± 5.2%; τ_{on}: 141 ± 16 ms) whereas the block of $\alpha_{1A/B(f)}$ was substantially slower and less complete (23.1 ± 3.0%, τ_{on}: 647 ± 286 ms; Fig. 9, *B–D*). The increase in ω-Aga IVA sensitivity after removal of amino acids $N^{1655}P^{1656}$ suggests that these two amino acids interfere with the interaction of ω-Aga IVA and a binding side in the IVS3-S4 linker. The role of this region for determining the ω-Aga IVA sensitivity is supported by the finding that the ω-Aga IVA sensitivity in $\alpha_{1A/B(f)}$ is further reduced, where NP and two additional neighboring amino acids are altered (IAET$^{1653–56}$, Fig. 4 *A*). However, an involvement of amino acids within the IVS5-SS1 region that are also altered in $\alpha_{1A/B(f)}$ cannot be ruled out.

In all cases, no relief from block by ω-Aga IVA was observed by extended wash with toxin-free saline (10–20 min) or by 10 strong depolarizations (50-ms depolarization to +130 mV, 1 Hz). With increase in number and frequency of strong depolarizations (50×, 10 Hz) we obtained 5 ± 1.9% ($n = 3$) relief from block for wt $\alpha_{1A\text{-}2}$ and $\alpha_{1A}\Delta$NP. In two experiments with $\alpha_{1A}\Delta$NP we applied four and five series of strong depolarizations (50×, 10 Hz) and obtained a cumulative relief of ~20 and 24%, respectively. The small relief of block observed here with $\alpha_{1A\text{-}2}$- or $\alpha_{1A}\Delta$NP-containing channels, even under conditions that allow prolonged channel openings at +130 mV, indicate a much higher affinity for ω-Aga IVA in the open state of the recombinant α_{1A} channel than that observed with native P-type Ca^{2+} channels (McDonough et al., 1997a).

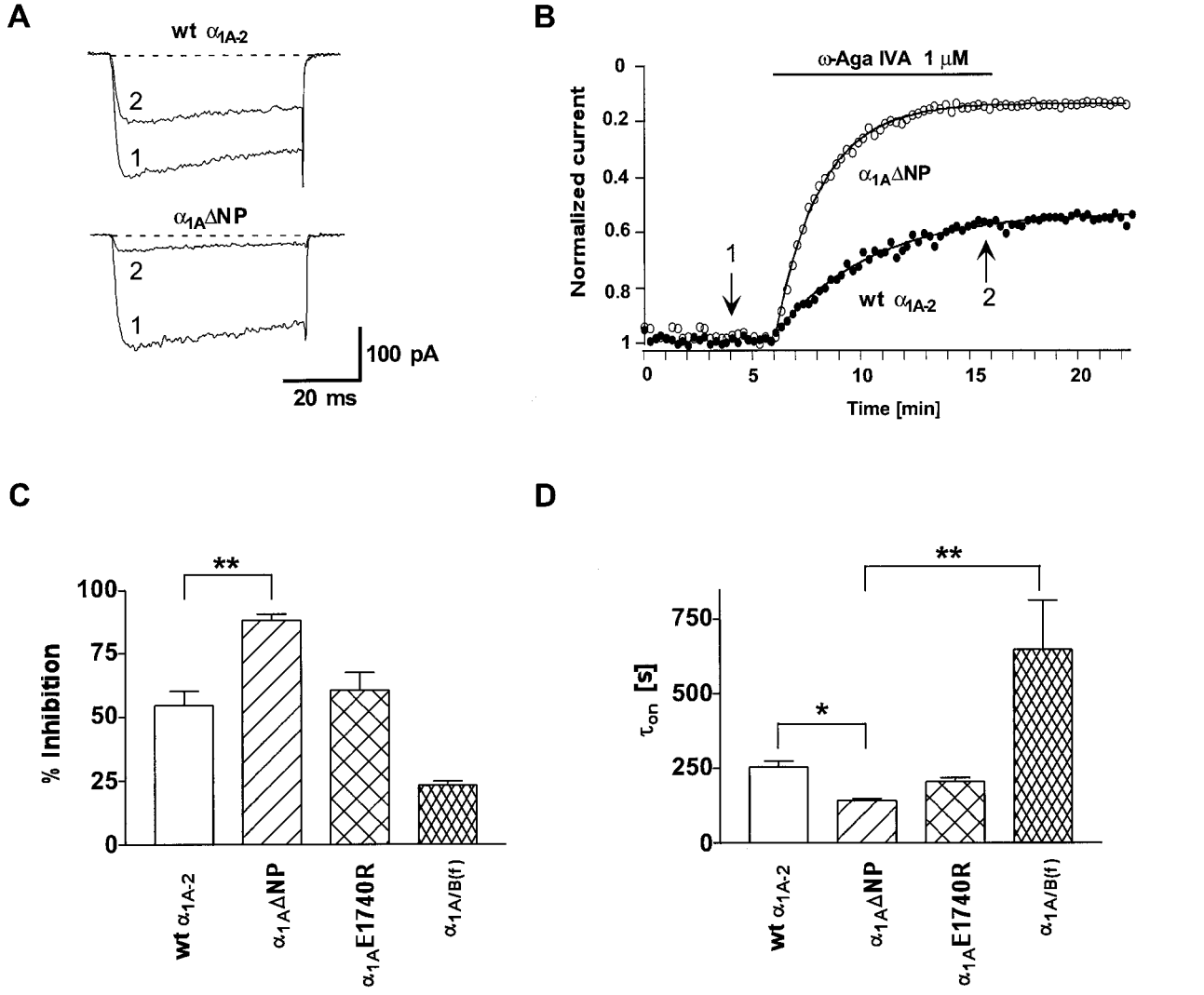

FIGURE 9 ω-Aga IVA inhibits α_{1A}ΔNP more potently than wt α_{1A}-containing channels. (*A*) Representative current traces from wt α_{1A-2} and α_{1A}ΔNP before (1) and 9.5 min after (2) application of 1 μM ω-Aga IVA. Currents were elicited by step-depolarizations to +10 mV from a holding potential of −90 mV. (*B*) Time course of inhibition of normalized Ba^{2+} current from wt α_{1A-2} (*open circles*) and α_{1A}ΔNP (*filled circles*). Horizontal bar: application of 1 μM ω-Aga IVA. The development of block followed an exponential function and the lines through the data points represent exponential fits with τ_{on} = 255 and 166 s for wt α_{1A-2} and α_{1A}ΔNP, respectively. The arrows indicate the time points for current shown in (*A*). (*C*) Maximum inhibition of Ba^{2+} currents by 1 μM ω-Aga IVA measured after a 10-min application of 1 μM ω-Aga IVA. (*D*) Comparison of τ_{on} for ω-Aga IVA block of wt and mutant channels. Values for τ_{on} were determined as illustrated in (*B*). Data points in (*C*) and (*D*) represent mean ± SE; wt α_{1A-2}, α_{1A}ΔNP, α_{1A}E1740R (n = 5), $\alpha_{1A/B(f)}$ (n = 3). * and **, values are significantly different at $p < 0.05$ and $p < 0.001$. All ω-Aga IVA-containing solutions also contained 1 mg/ml cytochrome *c*.

DISCUSSION

Cloning and biophysical properties of human α_{1A} Ca^{2+} channels

We have cloned two variants of the human α_{1A} Ca^{2+} channel subunit. The two forms arise from alternative splicing of human α_{1A} Ca^{2+} channel transcripts, resulting in a truncated COO^--terminus of the α_{1A-2} isoform relative to α_{1A-1}. Similar splicing has been observed with human BI (Zhuchenko et al., 1997), rabbit BI (Mori et al., 1991), and rat riA-1 (Ligon et al., 1998). Interestingly, the position of the five-nt deletion in the human α_{1A} that produces α_{1A-2} coincides with the position of the deletion in the human α_{1B-1} subunit that produces α_{1B-2} (Williams et al., 1992). The mutations within the human α_{1A} gene described by Ophoff et al. (1996) that have been associated with two neurological disorders, familial hemiplegic migraine and episodic ataxia type-2, are not present in the two α_{1A} isoforms described here. Both variants described here contain a two amino acid insert in the IVS3-S4 linker ($N^{1655}P^{1656}$) that dramatically affects the biophysical and pharmacological properties of the channel (see below). In the rat α_{1A} subunit, variants that contain the NP insert in the IVS3-S4 linker have been recently described for the neuronal (α_{1A-b}; Zamponi et al., 1996) and peripheral forms (Yu et al., 1992; Ligon et al., 1998). In contrast, they are not found in a human α_{1A} cDNA (Zhuchenko et al., 1997) or the genomic clones (Ophoff et al., 1996). Although one might

expect to find DNA sequence encoding the NP in the genomic sequence, it is possible that an additional exon encoding NP might be located in an as yet uncharacterized region. These findings suggest that the neuronal human α_{1A} variants described here represent a previously unidentified isoform of human α_{1A} and could represent a splice variation or a polymorphism of α_{1A}.

The biophysical properties of human $\alpha_{1A\text{-}2}$-containing Ca^{2+} channels are similar to those reported for the rat and rabbit homologs (Sather et al., 1993; Niidome et al., 1994; Stea et al., 1994; De Waard and Campbell, 1995). One of the most notable biophysical differences among human $\alpha_{1A\text{-}2}$, $\alpha_{1B\text{-}1}$, and $\alpha_{1E\text{-}3}$, each coexpressed with $\alpha_{2b}\delta$ and β_{1b} subunits, is that $\alpha_{1A\text{-}2}$-containing Ca^{2+} channels do not have appreciable holding potential sensitivity in ranges relevant to neurons (i.e., the $V_{1/2}$ of isochronal inactivation (20 s) is least negative for $\alpha_{1A\text{-}2}$-containing Ca^{2+} channels). Furthermore, the $\alpha_{1A\text{-}2}$-containing Ca^{2+} channels inactivate more slowly. Both $\alpha_{1B\text{-}1}$- and $\alpha_{1E\text{-}3}$-containing channels are more sensitive to changes in holding potential, and $\alpha_{1E\text{-}3}$-containing channels inactivate much more rapidly than $\alpha_{1A\text{-}2}$-containing channels. All three of these recombinant channels deactivate rapidly ($\leq$250 μs), consistent with their classification as HVA Ca^{2+} channels. This is also confirmed by the positive half-maximal voltage of activation of these three channels.

The half-maximal inactivation of the $\alpha_{1A\text{-}2}\alpha_{2b}\delta\beta_{1b}$ channels occurred at very positive potentials ($V_{1/2} = -17.4$ mV), indicating that these channels are most likely available for activation during periods of low and high action potential frequency in neurons. By comparison, P-type Ca^{2+} channels in rat cerebellar Purkinje cells or the rat α_{1A}-containing Ca^{2+} channels are somewhat more sensitive to holding potential ($V_{1/2} = -34$ and -30.4 mV, respectively; Regan et al., 1991; Berrow et al., 1997). Interestingly, $\alpha_{1A}\Delta$NP has a $V_{1/2}$ value (-37 mV) similar to that observed with rat cerebellar P-type Ca^{2+} channels. However, both the P-type and the human $\alpha_{1A\text{-}2}\alpha_{2b}\delta\beta_{1b}$ Ca^{2+} channel do not fully inactivate, with 10–15% residual current even at holding potentials of 0 mV or more positive. The $V_{1/2}$ of voltage-dependence of activation of the human α_{1A}-containing Ca^{2+} channel was nearly 30 mV more positive than the value obtained for the P-type Ca^{2+} channel (Regan et al., 1991). This difference may, in part, be explained by the higher external Ba^{2+} concentration used in the present study (15 mM vs. 5 mM).

α_{1A} chimeras and mutations in domain IV alter sensitivity to ω-Aga IVA

The block of human $\alpha_{1A\text{-}2}$-containing Ca^{2+} channels by ω-Aga IVA was less complete compared to rat cerebellar P-type Ca^{2+} channels (Mintz et al., 1992b; McDonough et al., 1997a) and was somewhat similar to that observed with recombinant rat α_{1A} expressed in COS-7 cells (Berrow et al., 1997). One of the structural differences between the human and rat α_{1A} subunit is the $N^{1555}P^{1556}$ insert in the IVS3-S4 extracellular linker in human α_{1A} that introduces an additional polar residue (N). Removal of these residues ($\alpha_{1A}\Delta$NP) significantly increased the amount and speed of block by ω-Aga IVA, whereas replacement of a charged residue within the IVS5-SS1 extracellular linker in the pore-forming region (E1740R) did not alter the toxin sensitivity. This suggests that the addition of the NP residues might sterically hinder the interaction of ω-Aga IVA with its binding site or weaken the interaction by providing an additional polar residue (N). This is consistent with the reduced ω-Aga IVA block observed with $\alpha_{1A/B(f)}$, which contains an additional polar and an additional charged residue to the IVS3-S4 linker (Fig. 4 *A*). However, $\alpha_{1A/B(f)}$ also contains amino acid changes in the IVS5-SS1 region, so it is possible that these residues also affect the interaction of ω-Aga IVA with the channel. Alternatively, the NP residues may cause an allosteric effect on the binding of ω-Aga IVA.

Residues within the IVS3-S4 linker have been shown to participate in binding of gating-modifier toxins to Na^+ (scorpion toxin; Rogers et al., 1996) and K^+ channels (hanatoxin; Swartz and MacKinnon, 1997b). Recently, Li-Smerin et al. (1998) showed that drk1 K^+ channels can also interact with the gating-modifier toxin grammotoxin, a potent P- and N-type Ca^{2+} channel inhibitor (McDonough et al., 1997a). Furthermore, binding of grammotoxin to drk1 K^+ channels can be greatly reduced by altering residues within the S3-S4 linker that also affect hanatoxin binding (Swartz and MacKinnon, 1997a, b), and conversely, the rabbit α_{1A} Ca^{2+} channel can be inhibited by hanatoxin, a selective K^+ channel blocker. Based on their findings, Li-Smerin et al. (1998) suggested that the S3-S4 linker contains a conserved voltage-sensing structure that is recognized by the gating modifier toxins. ω-Aga IVA has recently been shown to inhibit cerebellar P-type Ca^{2+} channels by modifying its gating mechanism (McDonough et al., 1997b). Our findings with $\alpha_{1A/B(f)}$ and $\alpha_{1A}\Delta$NP suggest that ω-Aga IVA might interact with residues in the IVS3-S4 linker in human α_{1A} that are homologous S3-S4 linker in drk1 K^+ channels. The differences in the amino acid composition of S3-S4 linker in the four domains of α_{1A} Ca^{2+} channels and the observation that grammotoxin binds to P-type Ca^{2+} channels in the presence of ω-Aga IVA (McDonough et al., 1997a) suggests that there are multiple heterogeneous toxin binding sites in α_{1A}. The selectivity of ω-Aga IVA for α_{1A} or P/Q-type Ca^{2+} channels suggests further differences in toxin binding sites between α_{1A} and α_{1B} Ca^{2+} channel. The reduction in ω-Aga IVA block observed with $\alpha_{1A/B(f)}$ suggests that key residues of the toxin binding site are located in IVS3-S4 linker (Fig. 4 *B*).

Localization of structural elements in domain IV involved in controlling current magnitude and inactivation

The two mutations in the $\alpha_{1A\text{-}2}$ subunit ($\alpha_{1A/B(f)}$, α_{1A}E1740R) that resulted in increased current magnitude

also resulted in a significant increase in the steady-state protein levels of α_1, $\alpha_{2b}\delta$, and β_{1b} subunits in cell membranes. This possibly reflects an increase in the stability of the complex within the membranes, the ability of the channel complex to incorporate into the plasma membrane, or the strength of the interaction among the subunits. The simplest explanation is that an increase in the number of channels in membranes results in an increased current magnitude. Increases in functional expression (or current magnitude) of Ca^{2+} channels containing rabbit α_{1C} or rat α_{1B} in *Xenopus* oocytes by alteration of the primary sequence of the α_1 subunit have been reported previously. Functional expression of recombinant Ca^{2+} channels was increased by partial deletion of the carboxyl terminus of the α_{1C} subunit or by partial exchange of the rat α_{1B} subunit amino terminus with the corresponding α_{1A} sequence (Wei et al., 1994; Ellinor et al., 1994). In the study by Ellinor et al. (1994) no data were presented to explain the effect; however, Wei et al. (1994) demonstrated that systematic deletions of increasing portions in the α_{1C} carboxy terminus resulted in an increase in current magnitude without changes in unitary conductance or charge movements during voltage-dependent gating, suggesting an increase in channel open probability rather than an increase in number of channels in the plasma membrane. This appears to be distinct from the results with α_{1A}E1740R and $\alpha_{1A/B(f)}$, as changes in amino acid sequence resulting in increased current magnitude involve amino acids located in the extracellular region of IVS3-IVSS1. Furthermore, in native cardiac L-type or recombinant human α_{1C}-containing Ca^{2+} channels, intracellular perfusion with proteolytic enzymes increased current magnitude (Hescheler and Trautwein, 1988; Klockner et al., 1995), a result similar to the enhancement observed with a carboxyl terminal deletion mutant of the α_{1C} subunit (Klockner et al., 1995; Wei et al., 1994). However, this mechanism may be specific to native cardiac L-type and recombinant α_{1C}-containing Ca^{2+} channels, as deletion of the carboxy terminus in a recombinant skeletal muscle α_{1S} subunit failed to enhance Ca^{2+} channel activity (Beam et al., 1992). In a similar manner, no change in the magnitude of Ba^{2+} currents was observed in the present study after substitution of the carboxy terminus of $\alpha_{1A\text{-}2}$ with the corresponding sequence of $\alpha_{1B\text{-}1}$. However, as none of the tested mutations, which accounted for the most dramatic differences in this region, resulted in the 30-fold increase in current magnitude as observed with $\alpha_{1A/B(f)}$, it is likely that a combination of any or all of these amino acid differences (81 possible combinations) may be necessary to achieve the changes observed with $\alpha_{1A/B(f)}$.

There are 20 amino acid differences between the $\alpha_{1A\text{-}2}$ and $\alpha_{1B\text{-}1}$ subunits in the 112 residue segment between IVS3 and IVSS1. All differences occur in two putative extracellular linkers next to the putative voltage sensor in the S4 segment: the IVS3-S4 and the IVS5-SS1 linker. Mutation in either one or both linker effected activation, inactivation kinetics, and channel availability, indicating that small changes in the local environment of the S4 segment are sufficient to significantly alter channel gating. Previous studies identified several structural elements within α_1 subunits that are involved in Ca^{2+} channel activation or inactivation. For example, channel activation has been associated with the IS3 segment and the IS3-S4 extracellular linker in α_{1S}-containing Ca^{2+} channels (Tanabe et al., 1991; Nakai et al., 1994), whereas regulation of voltage-dependent channel inactivation has been associated with the IS6 and flanking regions in α_{1B}-containing Ca^{2+} channels (Zhang et al., 1994), and the IIISS2-S6, IVS5-SS2, or the COO^- region in α_{1C}-containing Ca^{2+} channels (Yatani et al., 1994; Klockner et al., 1995). The findings with $\alpha_{1A/B(f)}$, $\alpha_{1A}\Delta$NP, and α_{1A}E1740R indicate the IVS3-S4 and IVS5-SS1 linkers contain structural elements involved in regulation of channel inactivation as well as activation.

Variation in the amino acid composition of the S3-S4 linker have previously been reported for N-type Ca^{2+} channels from rat brain in domain III (rbB-I, rbB-II; Dubel et al., 1994) and from superior cervical ganglion in domain IV (Lin et al., 1997). These variants might be the result of alternative splicing. Functional studies have shown that the variants that lack either a four amino acid insert in IIIS3-S4 (-SMTP, rbB-II) or a two amino acid insert in IVS3-S4 linker (-ET, rb$\alpha_{1B\text{-}d}$) activated and inactivated faster than the variants containing the corresponding inserts. Sequence alignment of the IVS3-S4 region from α_{1A} and α_{1B} reveals that the NP insert found in human α_{1A} occurs at a homologous position in rat α_{1B} (Fig. 4 *B*). These findings suggest that $\alpha_{1A}\Delta$NP may represent a genuine variant of human α_{1A} Ca^{2+} channels. Furthermore, the splice variation of the S3-S4 region(s) might be a general mechanism to control channel gating of α_{1A} or α_{1B} Ca^{2+} channels, and perhaps other voltage-gated channels. Changes in gating properties of α_{1A} or α_{1B} Ca^{2+} channels that control neurotransmitter release could significantly alter synaptic transmission, and therefore may have profound physiological consequences.

We thank Drs. S. Hess, M. Washburn, S. Madigan, and G. Veliçelebi for critical reading of the manuscript, P. Sionit for his excellent technical assistance and Pfizer (CT) for the generous gift of ω-Aga IVA. The GenBank access numbers for the $\alpha_{1A\text{-}2}$ and $\alpha_{1A\text{-}1}$ nucleotide sequences are AF004883 and AF004884, respectively.

REFERENCES

Beam, K. G., B. A. Adams, T. Niidome, S. Numa, and T. Tanabe. 1992. Function of a truncated dihydropyridine receptor as both voltage sensor and calcium channel. *Nature.* 360:169–171.

Berrow, N. S., N. L. Brice, I. Tedder, K. M. Page, and A. C. Dolphin. 1997. Properties of cloned rat α_{1A} calcium channels transiently expressed in the COS-7 cell line. *Eur. J. Neurosci.* 9:739–748.

Birnbaumer, L., K. P. Campbell, W. A. Catterall, M. M. Harpold, F. Hofmann, W. A. Horne, Y. Mori, A. Schwartz, T. P. Snutch, T. Tanabe, and R. W. Tsien. 1994. The naming of voltage-gated calcium channels. *Neuron.* 13:505–506.

Bleakman, D., D. Bowman, C. P. Bath, P. F. Brust, E. C. Johnson, C. R. Deal, R. J. Miller, S. B. Ellis, M. M. Harpold, M. Hans, and C. J.

Grantham. 1995. Characteristics of a human N-type calcium channel expressed in HEK293 cells. *Neuropharmacology.* 34:753–765.

Brust, P. F., S. Simerson, A. F. McCue, C. R. Deal, S. Schoonmaker, M. E. Williams, G. Velicelebi, E. C. Johnson, M. M. Harpold, and S. B. Ellis. 1993. Human neuronal voltage-dependent calcium channels: studies on subunit structure and role in channel assembly. *Neuropharmacology.* 32:1089–1102.

Catterall, W. A., K. de-Jongh, E. Rotman, J. Hell, R. Westenbroek, S. J. Dubel, and T. P. Snutch. 1993. Molecular properties of calcium channels in skeletal muscle and neurons. *Ann. NY Acad. Sci.* 681:342–355.

De Waard, M., and K. P. Campbell. 1995. Subunit regulation of the neuronal α_{1A} Ca^{2+} channel expressed in *Xenopus* oocytes. *J. Physiol.* 485:619–634.

Dubel, S. J., T. V. Starr, J. Hell, M. K. Ahlijanian, J. J. Enyeart, W. A. Catterall, and T. P. Snutch. 1992. Molecular cloning of the α_1 subunit of an ω-conotoxin-sensitive calcium channel. *Proc. Natl. Acad. Sci. USA.* 89:5058–5062.

Dubel, S. J., A. Stea, and T. P. Snutch. 1994. Two cloned rat brain N-type calcium channels have distinct kinetics. *Soc. Neurosci. Abstr.* 20:631.

Ellinor, P. T., J. F. Zhang, W. A. Horne, and R. W. Tsien. 1994. Structural determinants of the blockade of N-type calcium channels by a peptide neurotoxin. *Nature.* 372:272–275.

Fletcher, C. F., C. M. Lutz, T. N. O'Sullivan, J. D. Shaughnessy, Jr., R. Hawkes, W. N. Frankel, N. G. Copeland, and N. A. Jenkins. 1996. Absence epilepsy in tottering mutant mice is associated with calcium channel defects. *Cell.* 87:607–617.

Fujita, Y., M. Mynlieff, R. T. Dirksen, M. S. Kim, T. Niidome, J. Nakai, T. Friedrich, N. Iwabe, T. Miyata, and T. Furuichi. 1993. Primary structure and functional expression of the ω-conotoxin-sensitive N-type calcium channel from rabbit brain. *Neuron.* 10:585–598.

Gubler, U., and B. J. Hoffman. 1983. A simple and efficient method for generating cDNA libraries. *Gene.* 25:263–269.

Hamill, O. P., A. Marty, E. Neher, B. Sakmann, and F. J. Sigworth. 1981. Improved patch-clamp techniques for high-resolution current recording from cells and cell-free membrane patches. *Pflugers Arch.* 391:85–100.

Hescheler, J., and W. Trautwein. 1988. Modification of L-type calcium current by intracellularly applied trypsin in guinea-pig ventricular myocytes. *J. Physiol.* 404:259–274.

Hess, P. 1990. Calcium channels in vertebrate cells. *Annu. Rev. Neurosci.* 13:337–356.

Ho, S. N., H. D. Hunt, R. M. Horton, J. K. Pullen, and L. R. Pease. 1989. Site-directed mutagenesis by overlap extension using the polymerase chain reaction. *Gene.* 77:51–59.

Hofmann, F., M. Biel, and V. Flockerzi. 1994. Molecular basis for Ca^{2+} channel diversity. *Annu. Rev. Neurosci.* 17:399–418.

Kim, M. S., T. Morii, L. X. Sun, K. Imoto, and Y. Mori. 1993. Structural determinants of ion selectivity in brain calcium channel. *FEBS Lett.* 318:145–148.

Klockner, U., G. Mikala, G. Varadi, and A. Schwartz. 1995. Involvement of the carboxyl-terminal region of the α_1 subunit in voltage-dependent inactivation of cardiac calcium channels. *J. Biol. Chem.* 270: 17306–17310.

Lapeyre, B., and F. Amalric. 1985. A powerful method for the preparation of cDNA libraries: isolation of cDNA encoding a 100-kDa nuclear protein. *Gene.* 37:215–220.

Ligon, B., A. E. Boyd 3rd, and K. Dunlap. 1998. Class A calcium channel variants in pancreatic islets and their role in insulin secretion. *J. Biol. Chem.* 273:13905–13911.

Lin, Z., S. Haus, J. Edgerton, and D. Lipscombe. 1997. Identification of functionally distinct isoforms of the N-type Ca^{2+} channel in rat sympathetic ganglia and brain. *Neuron.* 18:153–166.

Li-Smerin, Y., and K. J. Swartz. 1998. Gating modifier toxins reveal a conserved structural motif in voltage-gated Ca^{2+} and K^+ channels. *Proc. Natl. Acad. Sci. USA*. 95:8585–8589.

Liu, H., M. De Waard, V. E. S. Scott, C. A. Gurnett, V. A. Lennon, and K. P. Campbell. 1996. Identification of three subunits of high affinity ω-conotoxin MVIIC-sensitive Ca^{2+} channel. *J. Biol. Chem.* 271: 13804–13810.

Llinas, R., M. Sugimori, D. E. Hillman, and B. Cherskey. 1992. Distribution and functional significance of P-type, voltage-dependent Ca^{2+} channels in mammalian central nervous system. *Trends Neurosci.* 5:351–355.

Matteson, D. R., and C. M. Armstrong. 1986. Properties of two types of calcium channels in clonal pituitary cells. *J. Gen. Physiol.* 87:161–182.

McDonough, S. I., R. A. Lampe, R. A. Keith, and B. P. Bean. 1997a. Voltage-dependent inhibition of N- and P-type calcium channels by the peptide toxin ω-grammotoxin-SIA. *Mol. Pharmacol.* 52:1095–1104.

McDonough, S. I., I. M. Mintz, and B. P. Bean. 1997b. Alteration of P-type calcium channel gating by the spider toxin ω-Aga-IVA. *Biophys. J.* 72:2117–2128.

Mintz, I. M., M. E. Adams, and B. P. Bean. 1992a. P-type calcium channels in rat central and peripheral neurons. *Neuron.* 9:85–95.

Mintz, I. M., V. J. Venema, K. M. Swiderek, T. D. Lee, B. P. Bean, and M. E. Adams. 1992b. P-type calcium channels blocked by the spider toxin ω-Aga-IVA. *Nature.* 355:827–829.

Mori, Y., T. Friedrich, M. S. Kim, A. Mikami, J. Nakai, P. Ruth, E. Bosse, F. Hofmann, V. Flockerzi, T. Furuichi, K. Mikoshiba, K. Imoto, T. Tanabe, and S. Numa. 1991. Primary structure and functional expression from complementary DNA of a brain calcium channel. *Nature.* 350: 398–402.

Nakai, J., B. A. Adams, K. Imoto, and K. G. Beam. 1994. Critical roles of the S3 segment and S3–S4 linker of repeat I in activation of L-type calcium channels. *Proc. Natl. Acad. Sci. USA*. 91:1014–1018.

Niidome, T., T. Teramoto, and K. Katayama. 1994. Stable and functional expression of rabbit brain BI calcium channel in baby hamster kidney cells. *Soc. Neurosci. Abstr.* 20:68.

Ophoff, R. A., G. M. Terwindt, M. N. Vergouwe, R. van Eijk, P. J. Oefner, S. M. Hoffman, J. E. Lamerdin, H. W. Mohrenweiser, D. E. Bulman, M. Ferrari, J. Haan, D. Lindhout, G. J. van Ommen, M. H. Hofker, M. D. Ferrari, and R. R. Frants. 1996. Familial hemiplegic migraine and episodic ataxia type-2 are caused by mutations in the Ca^{2+} channel gene CACNL1A4. *Cell.* 87:543–552.

Perez-Reyes, E., H. S. Kim, A. E. Lacerda, W. Horne, X. Y. Wei, D. Rampe, K. P. Campbell, A. M. Brown, and L. Birnbaumer. 1989. Induction of calcium currents by the expression of the α_1 subunit of the dihydropyridine receptor from skeletal muscle. *Nature.* 340:233–236.

Randall, A., and R. W. Tsien. 1995. Pharmacological dissection of multiple types of Ca^{2+} channel currents in rat cerebellar granule neurons. *J. Neurosci.* 15:2995–3012.

Regan, L. J., D. W. Sah, and B. P. Bean. 1991. Ca^{2+} channels in rat central and peripheral neurons: high-threshold current resistant to dihydropyridine blockers and ω-conotoxin. *Neuron.* 6:269–280.

Rogers, J. C., Y. Qu, T. N. Tanada, T. Scheuer, and W. A. Catterall. 1996. Molecular determinants of high affinity binding of α-scorpion toxin and sea anemone toxin in the S3–S4 extracellular loop in domain IV of the Na^+ channel α subunit. *J. Biol. Chem.* 271:15950–15962.

Sather, W. A., T. Tanabe, J. F. Zhang, Y. Mori, M. E. Adams, and R. W. Tsien. 1993. Distinctive biophysical and pharmacological properties of class A (BI) calcium channel α_1 subunits. *Neuron.* 11:291–303.

Snutch, T. P., and P. B. Reiner. 1992. Ca^{2+} channels: diversity of form and function. *Curr. Opin. Neurobiol.* 2:247–253.

Starr, T. V., W. Prystay, and T. P. Snutch. 1991. Primary structure of a Ca^{2+} channel that is highly expressed in the rat cerebellum. *Proc. Natl. Acad. Sci. USA.* 88:5621–5625.

Stea, A., W. J. Tomlinson, T. W. Soong, E. Bourinet, S. J. Dubel, S. R. Vincent, and T. P. Snutch. 1994. Localization and functional properties of a rat brain α_{1A} Ca^{2+} channel reflect similarities to neuronal Q- and P-type channels. *Proc. Natl. Acad. Sci. USA.* 91:10576–10580.

Swandulla, D., E. Carbone, and H. D. Lux. 1991. Do calcium channel classifications account for neuronal calcium channel diversity? *Trends Neurosci.* 14:46–51.

Swartz, K. J., and R. MacKinnon. 1997a. Hanatoxin modifies the gating of a voltage-dependent K^+ channel through multiple binding sites. *Neuron.* 18:665–673.

Swartz, K. J., and R. MacKinnon. 1997b. Mapping the receptor site for hanatoxin, a gating modifier of voltage-dependent K^+ channels. *Neuron.* 18:675–682.

Tanabe, T., B. A. Adams, S. Numa, and K. G. Beam. 1991. Repeat I of the dihydropyridine receptor is critical in determining Ca^{2+} channel activation kinetics. *Nature.* 352:800–803.

Tang, S., G. Mikala, A. Bahinski, A. Yatani, G. Varadi, and A. Schwartz. 1993. Molecular localization of ion selectivity sites within the pore of a human L-type cardiac Ca^{2+} channel. *J. Biol. Chem.* 268:13026–13029.

Tottene, A., A. Moretti, and D. Pietrobon. 1996. Functional diversity of P-type and R-type Ca^{2+} channels in rat cerebellar neurons. *J. Neurosci.* 16:6353–6363.

Tsien, R. W., P. T. Ellinor, and W. A. Horne. 1991. Molecular diversity of voltage-dependent Ca^{2+} channels. *Trends Pharmacol. Sci.* 12:349–354.

Wei, X., A. Neely, A. E. Lacerda, R. Olcese, E. Stefani, E. Perez-Reyes, and L. Birnbaumer. 1994. Modification of Ca^{2+} channel activity by deletions at the carboxyl terminus of the cardiac α_1 subunit. *J. Biol. Chem.* 269:1635–1640.

Westenbroek, R. E., T. Sakurai, E. M. Elliott, J. W. Hell, T. V. Starr, T. P. Snutch, and W. A. Catterall. 1995. Immunochemical identification and subcellular distribution of the α_{1A} subunits of brain Ca^{2+} channels. *J. Neurosci.* 15:6403–6418.

Williams, M. E., P. F. Brust, D. H. Feldman, S. Patthi, S. Simerson, A. Maroufi, A. F. McCue, G. Velicelebi, S. B. Ellis, and M. M. Harpold. 1992. Structure and functional expression of an ω-conotoxin-sensitive human N-type Ca^{2+} channel. *Science.* 257:389–395.

Williams, M. E., M. Hans, P. Sionit, E. C. Johnson, and S. B. Ellis. 1995. An essential structural domain that determines the biophysical properties of the human α_{1A} high-voltage activated Ca^{2+} channel. *Soc. Neurosci. Abstr.* 21:1282.

Williams, M. E., L. M. Marubio, C. R. Deal, M. Hans, P. F. Brust, L. H. Philipson, R. J. Miller, E. C. Johnson, M. M. Harpold, and S. B. Ellis. 1994. Structure and functional characterization of neuronal α_{1E} Ca^{2+} channel subtypes. *J. Biol. Chem.* 269:22347–22357.

Yang, J., P. T. Ellinor, W. A. Sather, J. F. Zhang, and R. W. Tsien. 1993. Molecular determinants of Ca^{2+} selectivity and ion permeation in L-type Ca^{2+} channels. *Nature.* 366:158–161.

Yatani, A., A. Bahinski, G. Mikala, S. Yamamoto, and A. Schwartz. 1994. Single amino acid substitutions within the ion permeation pathway alter single-channel conductance of the human L-type cardiac Ca^{2+} channel. *Circ. Res.* 75:315–323.

Yu, A. S., S. C. Hebert, B. M. Brenner, and J. Lytton. 1992. Molecular characterization and nephron distribution of a family of transcripts encoding the pore-forming subunit of Ca^{2+} channels in the kidney. *Proc. Natl. Acad. Sci. USA.* 89:10494–10498.

Zahl, N., S. Simerson, C. R. Deal, M. E. Williams, M. Hans, P. Prodanovich, A. McCue, P. Sionit, G. Velicelebi, P. F. Brust, E. C. Johnson, M. M. Harpold, and S. B. Ellis. 1994. Cloning and functional expression of human α_{1A} high voltage-activated Ca^{2+} channels. *Soc. Neurosci. Abstr.* 20:68.

Zamponi, G. W., T. W. Soong, E. Bourinet, and T. P. Snutch. 1996. Beta subunit coexpression and the α_1 subunit domain I-II linker affect piperidine block of neuronal Ca^{2+} channels. *J. Neurosci.* 16:2430–2443.

Zhang, J. F., P. T. Ellinor, R. W. Aldrich, and R. W. Tsien. 1994. Molecular determinants of voltage-dependent inactivation in Ca^{2+} channels. *Nature.* 372:97–100.

Zhuchenko, O., J. Bailey, P. Bonnen, T. Ashizawa, D. W. Stockton, C. Amos, W. B. Dobyns, S. H. Subramony, H. Y. Zoghbi, and C. C. Lee. 1997. Autosomal dominant cerebellar ataxia (SCA6) associated with small polyglutamine expansions in the α_{1A}-voltage-dependent Ca^{2+} channel. *Nat. Genet.* 15:62–69.